Simulating the Dynamics of a Thermal Cloud using Particle Methods

Andrew C. J. Wade

September 2009

A dissertation submitted in partial fulfillment for the degree of
Bachelor of Science with Honours in Physics

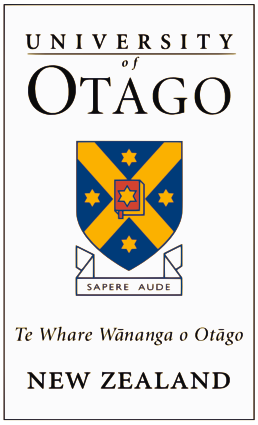

Abstract

We develop a Boltzmann equation solver for simulating the non-equilibrium dynamics of a therm cloud of Bosons. Our scheme, based on a particle and grid Monte Carlo approach, is efficient for simulating realistic experimental regimes.

We present numerous test of our algorithm and show results for the strongly non-equilibrium case of colliding thermal clouds.

Acknowledgements

There are some people I wish to thank..

I owe huge thanks to my supervisor Dr Blair Blakie, for huge amount of help when needed the most. Without his input this project could not have happened.

Dr Ashton Bradley for the discussions and advice.

My family for the support they have provided me.

All my fellow honors students for the invaluable discussions and good times!

Finally, Line Pedersen for the love, support and baking! She has provided me for many years.

Contents

Chapter 1

Introduction

Bose-Einstein Condensation (BEC) occurs when a single mode of a system becomes highly populated via Bose stimulated scattering. In this quantum state the particles lose their individual character and behave as single matter wave entity. This phenomenon was first predicted by Einstein in 1925 when he took Bose's work on photon statistics and applied it to atoms. BEC was finally achieved experimentally in 1995 when Cornell and Wieman at JILA [1] managed to condense approximately 2,000 rubidium atoms.

The dynamics of BEC are well described well in the low temperature limit (i.e. $T \ll T_c$, with T_c the critical temperature) by the Gross-Pitaevskii equation [2]. However, generalizing to finite temperature (i.e. $T \sim T_c$) has proved to be a challenging theoretical and computational problem. The Otago theory group has developed a powerful formalism for studying the finite temperature properties of a degenerate Bose gas known as c-field theory [3]. This formalism provides a complete dynamical description, but only for the low energy modes of the system. So far the description of the high energy modes has been restricted to a static mean field approach. This is a major limitation for the theory, which is alluded to in the work of Bezett and Blakie [4]. In this work they modelled the experiments of Jin *et al.* [5], in which a BEC system was perturbed and the m = 0 and m = 2 modes of oscillations are examined. Bezett and Blakie developed a projected Gross-Pitaevskii equation (PGPE) c-field description of these collective mode experiments. In this approach the system modes were divided into two regions, the **C** (classical field) and **I** (Incoherent) regions. By treating the **I**-region as being in static equilibrium, they found very good agreement with experiment at low temperatures, but fails to predict the sudden jump in the m = 0 mode frequency of the condensate and non-condensate at $T \approx 0.7\,T_c$. Stoof and co-workers [6, 7] suggested that this shift was due to the coupling of the in-phase and out-of-phase oscillations of the condensate and thermal cloud. Clearly a static **I**-region description is insufficient to capture this behaviour.

Other treatments by Jackson *et al.*[8] and Morgan *et al.*[9] have been able to predict the experimental results. The approach of Jackson was based on the Zaremba Nikuni Griffin formalism [10] (ZNG), which is similar to the c-field approach, although less general. In the ZNG approach, only the condensate itself is treated as a classical field and all excitations are treated semi-classically. As Jackson and Zaremba have made a successful numerical

implementation of a dynamical thermal cloud simulation, we use their work is an appropriate starting point for building a dynamical description of the **I**-region for the c-field theory.

While there is considerable expertise amongst the Otago c-field researchers in solving non-linear Schrödinger equations, there has been no on general Boltzmann simulations of thermal cloud dynamics. A major aim of this project is hence to develop the background techniques for simulating thermal cloud dynamics through a quantum Boltzmann equation.

To numerically implement the problem, I have closely followed the approach of Jackson and Zaremba. However, to develop the code for this implementation, a literature review of the derivation of the Boltzmann equation and particle/Monte Carlo (MC) techniques was conducted. This review allowed me to understand the surrounding issues, know-how, and techniques for these types of simulations. A particularly important issue I needed to address was why the equilibrium distribution appeared unaffected by collisions at the level of the Boltzmann equation. This issue, and its resolution, is discussed in Chapter 3. This literature review also enabled me to expand and discuss aspects of the Jackson and Zaremba implementation, which prove to be crucial in predicting the dynamics of the system simulated (e.g. density discussion in Appendix B leading to the non-physical damping seen in Chapter 5).

The original ZNG implementation of Jackson and Zaremba required supercomputer resources. Here we have aimed to develop efficient code with a view to running it (in parallel to the PGPE) on an ordinary workstation. Hence, I have suggested various possible improvement along the way and expanded on areas requiring more development.

With developing new code, it is required that many tests are performed to ensure the credibility of the outcomes of simulations. In Chapter 5 I present several applications of the code to problems which demonstrate validity and convergence. I also present two simulations showcasing what exciting non-equilibrium applications this code enables one to study.

A full non-equilibrium finite temperature theory is a major achievement. In this project we demonstrate the **I**-region component of such a theory. While a definitive scheme for coupling our Boltzmann equation/**I**-region solver to the c-field region has to be finalized, we speculate as to how this might be achieved.

Chapter 2

Background Theory

2.1 Setting the Scene for the Boltzmann Equation

Here we present a derivation of the classical Boltzmann equation suitable for our needs. This derivation has been influenced by our literature review of the books by Huang [12] and Kardar [13]. This background is necessary to understand and interpret the quantum Boltzmann equation derived by ZNG [10].

We consider a dilute cloud of distinguishable classical particles, i.e. the temperature is high enough and the density is low enough that the particles are localized wave packets with extensions much smaller than that of the average inter-particle distance. Further-more, we assume that they only interact via a differential cross-section, $\left|\frac{d\sigma}{d\Omega}\right|$.

Special attention is required when defining the distribution function $f(\mathbf{r}, \mathbf{p}, t)$, where

$$f(\mathbf{r}, \mathbf{p}, t) d^3r d^3p \tag{2.1}$$

tells us the number of particles contained in the phase-space volume $d^3r d^3p$ about the phase-space point $(\mathbf{r}, \mathbf{p})$. The phase-space volume elements d^3r and d^3p are not infinitesimals, but are finite volume elements. These volume elements are large enough that they contain many particles, but are small compared to macroscopic scales. If the phase-space density does not vary a lot from point to point, we may replace a sum over such volumes by an integral,

$$\sum f(\mathbf{r}, \mathbf{p}, t) d^3r d^3p = \int d^3r \int d^3p f(\mathbf{r}, \mathbf{p}, t). \tag{2.2}$$

We note that $f(\mathbf{r}, \mathbf{p}, t)$ is normalized such that when integrated over all phase-space it yields the total number of particles, N.

If there are no collisions, a particle found at the point $(\mathbf{r}, \mathbf{p})$ initially, will be found at the point $(\mathbf{r} + \frac{\mathbf{p}}{m}\delta t, \mathbf{p} + \mathbf{F}_{ext}(\mathbf{r}, t)\delta t)$ an infinitesimal time, δt, later. Here m is the mass of the particle and $\mathbf{F}_{ext}(\mathbf{r}, t)$ is the external force on the particle. Thus we may write

$$f(\mathbf{r} + \frac{\mathbf{p}}{m}\delta t, \mathbf{p} - \nabla_{\mathbf{r}} U_{ext}(\mathbf{r}, t)\delta t, t + \delta t) d^3r' d^3p' = f(\mathbf{r}, \mathbf{p}, t) d^3r d^3p, \tag{2.3}$$

where $U_{ext}(\mathbf{r},t)$ is the external potential and $d^3r'd^3p'$ is a volume element about $(\mathbf{r}+\frac{\mathbf{p}}{m}\delta t, \mathbf{p}-\nabla U_{ext}(\mathbf{r},t)\delta t)$.

Liouville's theorem[1] states that phase-space volume elements are constant under time evolution, i.e. $d^3rd^3p = d^3r'd^3p'$. This allows us to write

$$f(\mathbf{r}+\frac{\mathbf{p}}{m}\delta t, \mathbf{p}-\nabla_{\mathbf{r}}U_{ext}(\mathbf{r},t)\delta t, t+\delta t) = f(\mathbf{r},\mathbf{p},t) + \left(\frac{\partial f}{\partial t}\right)_{coll}\delta t, \tag{2.4}$$

where we have included also included collisions via an extra term, $\left(\frac{\partial f}{\partial t}\right)_{coll}\delta t$. This term quantifies the change in the number of particles over the interval δt, due to collisions with other particles. Expanding the left-hand-side of Eq. 2.4 about the point $(\mathbf{r},\mathbf{p},t)$ and letting $\delta t \to 0$, one finds the equation of motion for $f(\mathbf{r},\mathbf{p},t)$,

$$\left(\frac{\partial}{\partial t} + \frac{\mathbf{p}}{m}\cdot\nabla_{\mathbf{r}} - \nabla_{\mathbf{r}}U_{ext}(\mathbf{r},t)\cdot\nabla_{\mathbf{p}}\right) f(\mathbf{r},\mathbf{p},t) = \left(\frac{\partial f}{\partial t}\right)_{coll}. \tag{2.5}$$

For the above equation to be meaningful we need to determine the form of $\left(\frac{\partial f}{\partial t}\right)_{coll}$. To do this we make some assumptions about the system in question. One such assumption is that our system is dilute enough such that only binary collisions occur. We will discuss elastic binary collisions shortly, but first allow us to recast $\left(\frac{\partial f}{\partial t}\right)_{coll}$ in a more useful form.

Making the definitions,

$$R_{out}(\mathbf{r},\mathbf{p},t)\delta t d^3rd^3p = \begin{array}{l}\text{No. of collisions occuring during the time}\\ \text{interval } t \text{ to } t+\delta t, \text{ which one of the } \textit{initial}\\ \text{particles is in } d^3rd^3p \text{ about } (\mathbf{r},\mathbf{p}).\end{array} \tag{2.6}$$

$$R_{in}(\mathbf{r},\mathbf{p},t)\delta t d^3rd^3p = \begin{array}{l}\text{No. of collisions occuring during the time}\\ \text{interval } t \text{ to } t+\delta t, \text{ which one of the } \textit{final}\\ \text{particles is in } d^3rd^3p \text{ about } (\mathbf{r},\mathbf{p}).\end{array} \tag{2.7}$$

and taking $R_{out}(\mathbf{r},\mathbf{p},t)d^3rd^3p$ and $R_{in}(\mathbf{r},\mathbf{p},t)d^3rd^3p$ to be the rates at which particles scatter into and out of the phase-space volume element d^3rd^3p about $(\mathbf{r},\mathbf{p})$, respectively. With the these definitions, we make the error in neglecting that the possibility the collision partner may also satisfy these conditions. However, the number of collision partners for which this is true is negligible, since d^3p is small.

This allows us to write,

$$\left(\frac{\partial f}{\partial t}\right)_{coll}\delta t = (R_{in}-R_{out})\delta t. \tag{2.8}$$

2.2 Elastic Binary Collisions

Here we consider the case of an elastic collision of two classical, spin-less, free particles of equal mass. This also applies to the case of two particles in some external potential, provided

[1] A simple proof can be found on pages 59-60 of [13].

that the differential cross-section is not effected by the external potential (i.e. the interaction length scale is much shorter than the length scale over which the external potential varies).

For conservation of momentum and energy we require that

$$\begin{aligned} \mathbf{P} &= \mathbf{P}', \\ |\mathbf{u}| &= |\mathbf{u}'|, \end{aligned} \tag{2.9}$$

where

$$\begin{aligned} \mathbf{P} &= \frac{1}{2}(\mathbf{p}_1 + \mathbf{p}_2), \\ \mathbf{u} &= \mathbf{p}_2 - \mathbf{p}_1, \end{aligned} \tag{2.10}$$

with $\mathbf{p}_1$ and $\mathbf{p}_2$ the initial momenta of the particles and the primes indicate final momenta. These equations tell us that the effect of the collision is to rotate the relative momentum, $\mathbf{u}$,

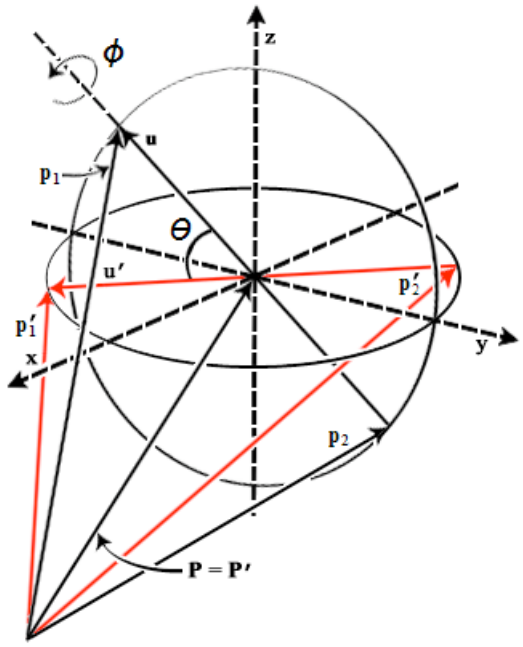

Figure 2.1: Geometrical representation of a binary collision.

about the point $\mathbf{P}$, see Fig. 2.1. If we know the scattering angles θ and ϕ, shown in Fig. 2.1, the collision is completely characterised.

While holding θ and ϕ fixed and varying $\mathbf{P}$ and $\mathbf{u}$ slightly to $\mathbf{P} + d\mathbf{P}$ and $\mathbf{u} + d\mathbf{u}$, respectively, one can show $d^3P d^3u = d^3P' d^3u'$. It follows from Eqs. 2.10 that $d^3v_1 d^3v_2 = d^3v_1' d^3v_2'$. This equality becomes important to us later in Section 2.3. However, what concerns us the most here is that elastic collisions simply rotate the relative momentum in a fashion that the final momenta of the particles lie on a sphere of radius $\frac{|\mathbf{u}|}{2}$, centred at $\mathbf{P}$.

The initial momenta of the two particles alone are not enough to determine the scattering angles. We also require the *impact parameter*, b, which is illustrated in Fig. 2.2. The

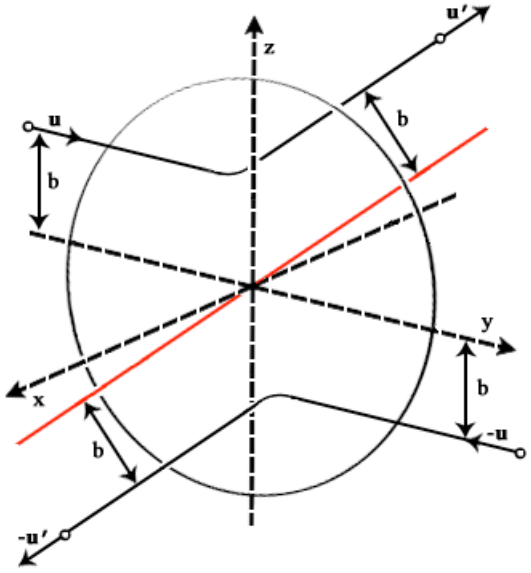

Figure 2.2: Binary Collision: Centre of Mass Frame.

collision in Fig. 2.2 is shown in the centre of mass frame, which is obtained by translating the coordinate system with the uniform momentum $-\mathbf{P}$. The two particles in Fig. 2.2 are travelling along the collision axis (y axis) with the relative momentum, $\mathbf{u}$. We see that the impact parameter is the perpendicular distance from the collision axis to the particles.

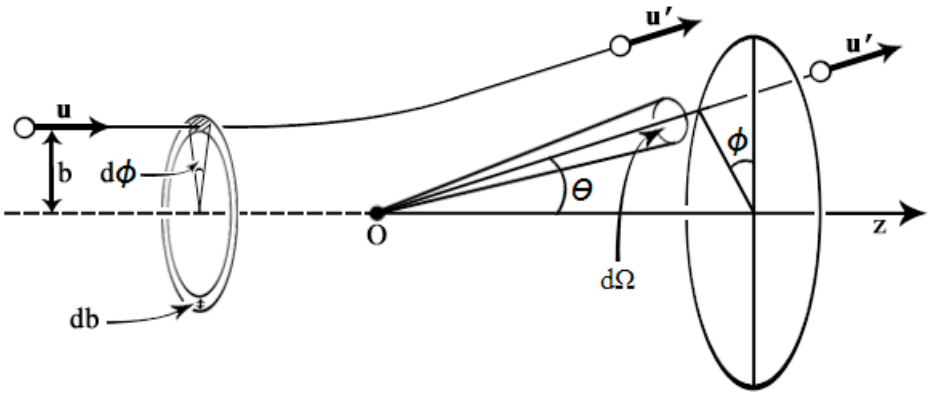

Figure 2.3: Scattering of particle about some origin O.

The differential cross-section, $\left|\frac{d\sigma}{d\Omega}\right|$, is defined as the Jacobian for the transform of variables $(b, \phi) \rightarrow \Omega$, where Ω is the solid angle seen in Fig. 2.3. This requires a one-to-one correspondence for the variables, i.e. for any given b and ϕ, a single output trajectory is given. The differential cross-section is the area presented to an incoming beam of particles, which scatter into the solid angle Ω. Fig. 2.3 accentuates the fact that we need only concern ourselves with one of the collision partners, since the other moves oppositely (also see

Fig. 2.2).

The details of the differential cross-section depends on the nature of the interaction potential and in general can depend on the relative momentum of the particles. However, there are some symmetry properties which are true in general, owing to interactions being electromagnetic in nature.

$$\left|\frac{d\sigma}{d\Omega}\right| = \begin{cases} \text{Invariant under time reversal.} \\ \text{Invariant under rotation and reflection.} \end{cases} \tag{2.11}$$

The second of the invariance properties 2.11 leads to the fact that the inverse collision has the same differential cross-section.

2.3 Boltzmann Equation

We now aim to find an equation for $\left(\frac{\partial f}{\partial t}\right)_{coll}$ in terms of the formalism we developed in Section 2.2, giving us the Boltzmann equation.

To obtain the Boltzmann equation we make the following approximations.

1. Only binary collisions are taken into account.
2. The effect of the external potential on $\left|\frac{\mathrm{d}\sigma}{\mathrm{d}\Omega}\right|$ can be neglected. (2.12)
3. The momentum of a particle is uncorrelated with its position.

It has already been mentioned that the first approximation of 2.12 is valid provided the cloud is dilute enough. Approximation 3 is known as the assumption of molecular chaos. This assumption allows us to write the number of particles in the same spatial volume d^3r about the point $\mathbf{r}$ with momentum in the volumes d^3p_1 and d^3p_2 about the points $\mathbf{p}_1$ and $\mathbf{p}_2$, respectively, as

$$\left[f(\mathbf{r},\mathbf{p}_1,t)d^3rd^3p_1\right]\left[f(\mathbf{r},\mathbf{p}_2,t)d^3rd^3p_2\right]. \tag{2.13}$$

The flux of particles with momentum in the volume d^3p_2 about $\mathbf{p}_2$, $I(\mathbf{r},\mathbf{p}_1,\mathbf{p}_2,t)$, impinging on a single particle that has momentum $\mathbf{p}_1$, is given by the number of particles in that volume (d^3p_2), multiplied by their relative speed.

$$I(\mathbf{r},\mathbf{p}_1,\mathbf{p}_2,t) = f(\mathbf{r},\mathbf{p}_2,t)d^3p_2\frac{|\mathbf{p}_2-\mathbf{p}_1|}{m}. \tag{2.14}$$

Thus, number of collisions due to this incoming flux that scatter into the solid angle $d\Omega$ during the time interval δt, is given by

$$Ibdbd\phi\delta t = I\left|\frac{d\sigma}{d\Omega}\right|d\Omega\delta t = f(\mathbf{r},\mathbf{p}_2,t)d^3p_2\frac{|\mathbf{p}_2-\mathbf{p}_1|}{m}\left|\frac{d\sigma}{d\Omega}\right|d\Omega\delta t. \tag{2.15}$$

Multiplying this expression by the number of particles with momentum $\mathbf{p}_1$ in the volume $d^3p_1d^3r$ at the point $\mathbf{r}$ and integrating over all $\mathbf{p}_2$ and Ω, we obtain the total number of collisions for the particles in the volume $d^3p_1d^3r$ at the point $(\mathbf{r},\mathbf{p}_1)$. Here we are assuming

that the effective range of the interaction potential is within d^3r.[2] This, by the definition 2.6, gives us

$$R_{out}(\mathbf{r},\mathbf{p}_1,t)\delta t = f(\mathbf{r},\mathbf{p}_1,t)\left[\int d\Omega \int d^3p_2 f(\mathbf{r},\mathbf{p}_2,t)\frac{|\mathbf{p}_2-\mathbf{p}_1|}{m}\left|\frac{d\sigma}{d\Omega}\right|\right]\delta t. \tag{2.16}$$

We reiterate that we may use $f(\mathbf{r},\mathbf{p}_1,t)$ and $f(\mathbf{r},\mathbf{p}_2,t)$ from the assumption of molecular chaos.

With a similar discussion for the inverse process one can find

$$R_{in}(\mathbf{r},\mathbf{p}_1,t)d^3p_1\delta t = f(\mathbf{r},\mathbf{p}_1',t)d^3p_1'\left[\int d\Omega \int d^3p_2' f(\mathbf{r},\mathbf{p}_2',t)\frac{|\mathbf{p}_2'-\mathbf{p}_1'|}{m}\left|\frac{d\sigma'}{d\Omega}\right|\right]\delta t. \tag{2.17}$$

From Section 2.2 we have the following relations,

$$\begin{aligned} |\mathbf{u}| = |\mathbf{p}_2-\mathbf{p}_1| = |\mathbf{u}'| = |\mathbf{p}_2'-\mathbf{p}_1'|\,, \\ d^3v_1d^3v_2 = d^3v_1'd^3v_2', \\ \left|\frac{d\sigma}{d\Omega}\right| = \left|\frac{d\sigma'}{d\Omega}\right|, \end{aligned} \tag{2.18}$$

allowing us to write (remembering that $\mathbf{p}_1'$ and $\mathbf{p}_2'$ are functions of $\mathbf{p}_1$, $\mathbf{p}_2$, and Ω),

$$\left(\frac{\partial f}{\partial t}\right)_{coll} = R_{in}-R_{out} = \int d\Omega \int d^3p_2 \frac{|\mathbf{p}_2-\mathbf{p}_1|}{m}\left|\frac{d\sigma}{d\Omega}\right|[f(\mathbf{r},\mathbf{p}_1',t)f(\mathbf{r},\mathbf{p}_2',t) - f(\mathbf{r},\mathbf{p}_1,t)f(\mathbf{r},\mathbf{p}_2,t)]\,. \tag{2.19}$$

Finally combining Eqs. 2.5 and 2.19 we obtain the Boltzmann equation,

$$\left(\frac{\partial}{\partial t}+\frac{\mathbf{p}}{m}\cdot\nabla_{\mathbf{r}}-\nabla_{\mathbf{r}}U_{ext}(\mathbf{r},t)\cdot\nabla_{\mathbf{p}}\right)f(\mathbf{r},\mathbf{p},t) = \int d\Omega\int d^3p_2\frac{|\mathbf{p}_2-\mathbf{p}|}{m}\left|\frac{d\sigma}{d\Omega}\right|\times [f(\mathbf{r},\mathbf{p}',t)f(\mathbf{r},\mathbf{p}_2',t)-f(\mathbf{r},\mathbf{p},t)f(\mathbf{r},\mathbf{p}_2,t)]\,. \tag{2.20}$$

It is useful at this point to summarize the above derivation by describing what Eq. 2.20 tells us. The left-hand-side of the equation contains the so called streaming terms. These describe the evolution of a single particle in some external potential $U_{ext}(\mathbf{r},t)$. The first of the streaming terms updates time, the second updates the position of the particle, and the last term updates the momentum of the particle. The collision integral on the right-hand-side tells us that the probability of finding a particle with momentum $\mathbf{p}$ and position $\mathbf{r}$ is suddenly altered if it undergoes a collision. The probability of such a collision is dependent on the flux of particles impinging on the particle and the differential cross-section. To say this another way, the probability of such a collision is dependent on some kinetic factors and the

[2] Otherwise, while we integrate over all impact parameters, we are integrating outside of the volume d^3r. If this was the case, we should be using the expression $f(\mathbf{r}(\Omega),\mathbf{p}_2,t)$ for the phase-space density.

probability of finding two particles at the point, which we approximated as $f(\mathbf{r},\mathbf{p},t)f(\mathbf{r},\mathbf{p}_2,t)$ (assumes position and momentum are uncorrelated). The first term in the collision integral, $f(\mathbf{r},\mathbf{p}',t)f(\mathbf{r},\mathbf{p}_2',t)$, describes the reverse scattering process, which increases the phase-space density at $(\mathbf{r},\mathbf{p})$. The other describes the scattering process where one of the initial particles scatters out of the phase-space point in question, hence, decreasing the density.

2.4 ZNG Equation of Motion for the Condensate

A numerical implementation of a Boltzmann equation solver for thermal cloud dynamics has been provided by Jackson and Zaremba in their application of the ZNG formalism [11]. We review the basics of this formalism here for completeness.

Effectively the ZNG theory couples the thermal cloud dynamics directly to the evolution of a Gross-Pitaevskii equation for the condensate. Future extension of the work here will be to couple our Boltzmann equation solver to the Otago c-field theory. This differs from the ZNG case in a few details, which may require additional work.

The content of this section and the next are taken from our literature review of the works of Dalfovo and Giorgini [2], and Zaremba and coworkers [10, 11]. In Section 2.5 Zaremba and coworkers follow the work of Kirkpatrick and Dorfman [15], the difference being that the equation of motion for the thermal cloud found in [10] is for the lab frame, whereas Kirkpatrick and Dorfman work in the local rest frame.

The second quantized, many body Hamiltonian for bosons is given by

$$\hat{H} = \int d^3r \hat{\Psi}^\dagger(\mathbf{r}) \left[-\frac{\hbar^2}{2m}\nabla^2_{\mathbf{r}} + U_{ext}(\mathbf{r}) \right] \hat{\Psi}(\mathbf{r}) + \frac{1}{2}\int d^3r d^3r_2 \hat{\Psi}^\dagger(\mathbf{r})\hat{\Psi}^\dagger(\mathbf{r}_2) V_{int}(\mathbf{r}-\mathbf{r}_2)\hat{\Psi}(\mathbf{r}_2)\hat{\Psi}(\mathbf{r}), \tag{2.21}$$

where $\hat{\Psi}^\dagger(\mathbf{r})$ and $\hat{\Psi}(\mathbf{r})$ are the boson field operators, $U_{ext}(\mathbf{r})$ is some external potential, and $V_{int}(\mathbf{r}-\mathbf{r}_2)$ is the two-body interaction potential. While working in the Heisenberg picture, we can decompose the field operator, $\hat{\Psi}(\mathbf{r},t)$, into two parts.

$$\hat{\Psi}(\mathbf{r},t) = \Phi(\mathbf{r},t) + \tilde{\Psi}(\mathbf{r},t). \tag{2.22}$$

The classical field, $\Phi(\mathbf{r},t)$, is the expectation value of the field operator, i.e. $\Phi(\mathbf{r},t) = \left\langle \hat{\Psi}(\mathbf{r},t) \right\rangle$. The modulus of $\Phi(\mathbf{r},t)$ gives the condensate density, $n_c(\mathbf{r},t) = |\Phi(\mathbf{r},t)|^2$. The operator $\tilde{\Psi}(\mathbf{r},t)$ describes the atoms outside the condensate, i.e. those in the thermal cloud.

Using the Heisenberg equation of motion one obtains the equation of motion for the field operator.

$$i\hbar\frac{\partial\hat{\Psi}(\mathbf{r},t)}{\partial t} = \left[\hat{\Psi}(\mathbf{r},t),\hat{H}\right] = \left(-\frac{\hbar^2}{2m}\nabla^2_{\mathbf{r}} + U_{ext}(\mathbf{r})\right)\hat{\Psi}(\mathbf{r},t) + g\hat{\Psi}^\dagger(\mathbf{r},t)\hat{\Psi}(\mathbf{r},t)\hat{\Psi}(\mathbf{r},t). \tag{2.23}$$

It has been assumed that we may replace the interaction potential by a pseudo potential $V_{int}(\mathbf{r}-\mathbf{r}_2) \to g\delta(\mathbf{r}-\mathbf{r}_2)$, where g is the strength of the interaction and it is related to the s-wave scattering length, a, by $g = \frac{4\pi\hbar^2 a}{m}$.

Taking the expectation value of Eq. 2.23 and making use of the Popov approximation[3], one finds a generalized form of the Gross-Pitaevskii equation.

$$i\hbar\frac{\partial\Phi(\mathbf{r},t)}{\partial t} = \left(-\frac{\hbar^2\nabla^2_{\mathbf{r}}}{2m} + U_{ext}(\mathbf{r}) + g\left[n_c(\mathbf{r},t) + 2\tilde{n}(\mathbf{r},t)\right] - iR(\mathbf{r},t)\right)\Phi(\mathbf{r},t), \tag{2.24}$$

where $n_t(\mathbf{r},t) = \left\langle\tilde{\Psi}^\dagger(\mathbf{r},t)\tilde{\Psi}(\mathbf{r},t)\right\rangle$ is the thermal cloud density. The source term $R(\mathbf{r},t)$ arises from the three-field correlation function $\left\langle\tilde{\Psi}^\dagger(\mathbf{r},t)\tilde{\Psi}(\mathbf{r},t)\tilde{\Psi}(\mathbf{r},t)\right\rangle$, which describes the transfer of atoms between the thermal cloud and the condensate. An equation for this term is defined in the following section.

2.5 ZNG Quantum Boltzmann Equation for the Thermal Cloud

Using Eqs. 2.23, 2.22, and a variation of Eq. 2.24 [10], one can come to an equation of motion for the thermal cloud field operator (suppressing arguments for convenience).

$$i\hbar\frac{\partial\tilde{\Psi}}{\partial t} = \left(-\frac{\hbar^2}{2m}\nabla^2_{\mathbf{r}} + U_{ext}\right)\tilde{\Psi} - 2gn_t\tilde{\Psi} + g\Phi^2\tilde{\Psi}^\dagger + g\Phi*(\tilde{\Psi}\tilde{\Psi} - \tilde{m}) + 2g\Phi(\tilde{\Psi}^\dagger\tilde{\Psi} - n_t) + g\left(\tilde{\Psi}^\dagger\tilde{\Psi}\tilde{\Psi} - \left\langle\tilde{\Psi}^\dagger\tilde{\Psi}\right\rangle\right). \tag{2.25}$$

Using the Wigner operator ([26]) to describe the dynamics of the thermal cloud as well as various other methods and approximations [10], one can reduce Eq. 2.25 to a quantum Boltzmann equation for the thermal cloud.

$$\left(\frac{\partial}{\partial t} + \frac{\mathbf{p}}{m}\cdot\nabla_{\mathbf{r}} - \nabla_{\mathbf{r}}U(\mathbf{r},t)\cdot\nabla_{\mathbf{p}}\right)f(\mathbf{r},\mathbf{p},t) = C_{12}[f] + C_{22}[f]. \tag{2.26}$$

To arrive at this equation requires a significant amount of work[4], which will not be reproduced here. The phase-space distribution, $f(\mathbf{r},\mathbf{p},t)$, is defined via the Wigner operator and knowledge of this function allows one to calculate various expectation values with it.

The thermal cloud is assumed to be well described semi-classically, with coordinates of position, momentum, and energy $\epsilon = \frac{p^2}{2m} + U(\mathbf{r},t)$, where $U(\mathbf{r},t)$ is the effective potential,

$$U(\mathbf{r},t) = U_{ext}(\mathbf{r}) + 2g\left[n_c(\mathbf{r},t) + n_t(\mathbf{r},t)\right], \tag{2.27}$$

including the Hartree-Fock meanfield terms.

The thermal cloud density may be expressed in terms of $f(\mathbf{r},\mathbf{p},t)$ by the following,

$$n_t(\mathbf{r},t) = \int\frac{d^3p}{h^3}f(\mathbf{r},\mathbf{p},t). \tag{2.28}$$

[3]Neglect the "anomalous" density $\tilde{m}(\mathbf{r},t) = \left\langle\tilde{\Psi}(\mathbf{r},t)\tilde{\Psi}(\mathbf{r},t)\right\rangle$.

[4]See Section 3 and Appendix A. of [11].

The collision integral, $C_{12}[f]$, appearing in Eq. 2.26 describes collisions which involve condensate atoms with the thermal cloud atoms and the $C_{22}[f]$ collision integral describes collisions which only involve the thermal cloud atoms.

The collision integral, $C_{22}[f]$, is given by

$$C_{22}[f] = \frac{\sigma}{\pi h^3 m^2} \int d^3p_2 \int d^3p_3 \int d^3p_4 \delta(\mathbf{p} + \mathbf{p}_2 - \mathbf{p}_3 - \mathbf{p}_4)\delta(\epsilon + \epsilon_2 - \epsilon_3 - \epsilon_4)\times \\ [(1+f)(1+f_2)f_3 f_4 - f f_2(1+f_3)(1+f_4)]\,, \quad (2.29)$$

where σ is the total bosonic cross-section, $\sigma = 8\pi a^2$. We have adopted the notation $f = f(\mathbf{p}, \mathbf{r}, t)$ and $f_i = f(\mathbf{p}_i, \mathbf{r}, t)$. Eq. 2.29 has a simple interpretation of which mirrors the interpretation of the classical Boltzmann equation: The two delta functions ensure conservation of energy and momentum for the collision[5], while the terms involving the phase-space distribution describe which collision process is occurring. For example $(1+f)(1+f_2)f_3 f_4$ describes two thermal cloud atoms colliding and one of the final states contributes to $f(\mathbf{p}, \mathbf{r}, t)$. The probability of such a scattering is now effected by the bosonic nature of the atoms (Bose stimulated scattering). In the sense that the atoms are encouraged to scatter into states which are already occupied. This manifests itself in Eq. 2.29 via the Bose enhancement terms $(1+f)(1+f_2)$ and $(1+f_3)(1+f_4)$. For the sake of comparison Eq. 2.29 can be rewritten when using the ideas of Section 2.2, as the following.

$$C_{22}[f] = \int \frac{d^3p_2}{h^3} \int \frac{d\Omega}{4\pi} \sigma \frac{|\mathbf{p}_2 - \mathbf{p}|}{m} [(1+f)(1+f_2)f_3 f_4 - f f_2(1+f_3)(1+f_4)]\,. \quad (2.30)$$

We see that Eq. 2.30 has strikingly similar structure to the collision integral in Eq. 2.20, only it contains contributions from our knowledge of quantum mechanics (i.e. Bose scattering and low energy collisions).

The collision term $C_{12}[f]$ is given by

$$C_{12}[f] = \frac{\sigma}{\pi h^3 m^2} \int d^3p_2 \int d^3p_3 \int d^3p_4 \delta(m\mathbf{v}_c + \mathbf{p}_2 - \mathbf{p}_3 - \mathbf{p}_4)\delta(\epsilon_c + \epsilon_2 - \epsilon_3 - \epsilon_4)\times \\ [\delta(\mathbf{p} - \mathbf{p}_2) - \delta(\mathbf{p} - \mathbf{p}_3) - \delta(\mathbf{p} - \mathbf{p}_4)]\times \\ [n_c(1+f_2)f_3 f_4 - n_c f_2(1+f_3)(1+f_4)]\,, \quad (2.31)$$

where the local condensate velocity, $\mathbf{v}_c$, and energy, ϵ_c, are given by

$$\mathbf{v}_c(\mathbf{r}, t) = \frac{\hbar}{2im|\Phi|^2} [\Phi^* \nabla_{\mathbf{r}} \Phi - \Phi \nabla_{\mathbf{r}} \Phi^*] \quad (2.32)$$

$$\epsilon_c = \frac{1}{2} m v_c^2 + \mu_c. \quad (2.33)$$

We see the condensate chemical potential appearing here, which is given by

$$\mu_c = -\frac{\hbar^2}{2m} \frac{\nabla_{\mathbf{r}}^2 \sqrt{n_c}}{\sqrt{n_c}} + U_{ext} + g n_c + 2 g n_t. \quad (2.34)$$

[5]We note that in the pseudo potential approximation, which is valid for the low energy collisions in these ultracold gases, the differential cross-section is momentum independent.

Again, Eq. 2.31 has a simple interpretation. In collisions which involve the condensate there are two possible outcomes that are encapsulated by the delta functions $[\delta(\mathbf{p}-\mathbf{p}_2)-\delta(\mathbf{p}-\mathbf{p}_3)-\delta(\mathbf{p}-\mathbf{p}_4)]$. The first delta function describes the process where a thermal atom collides with an atom in the condensate, ejecting the condensate atom into the thermal cloud. The others describe the process where one of the two initial thermal atoms, after the collision is found in the condensate. The sign of the delta functions changes the signs of the terms $[n_c(1+f_2)f_3f_4 - n_c f_2(1+f_3)(1+f_4)]$ such that these terms have the correct sign for collision described by the delta function (i.e. if the collision increase the phase-space density, the corresponding term is of positive sign).

The $C_{12}[f]$ collision integral acts as the mechanism to transfer atoms between the condensate and thermal cloud. Hence, we have

$$R(\mathbf{r},t) = \frac{\hbar}{2n_c}\int \frac{d^3p}{h^3} C_{12}[f]\,. \tag{2.35}$$

We see that the equations of motion for the condensate (Eq. 2.24) and thermal cloud (Eq. 2.26) are coupled via the collision integral, $C_{12}[f]$, and the densities of the condensate and thermal cloud.

In this section you may have noticed that the structure of the classical Boltzmann equation and the quantum Boltzmann equation do not quite agree. In the classical Boltzmann equation the only contribution from the interaction potential is the collision integral. This is not the case for the quantum Boltzmann equation. We see contributions in the form of the HF mean field, as well as, the collision integrals. This observation is addressed in Chapter 3.

2.6 Introduction to Discrete Particle Methods

The purpose of this section is to survey the standard approaches used for discrete particle simulations. These methods are commonly used for simulations in the areas of plasma physics, semiconductors, and astrophysics. Two useful references for this section are the text by Hockney and Eastwood [16] and the text by Birdsall and Langdon [19].

2.6.1 Particle Force Models

In all particle simulations one must calculate the forces between particles in order to propagate the particles through space. The method used to calculate these forces generally falls into one of the three categories, Particle-Particle (PP), Particle-Mesh (PM), and Particle-Particle-Particle-Mesh (P^3M) Methods.

2.6.1.1 Particle-Particle Method

The PP method is simplest model and most direct for calculating forces. At each time step of the simulation, for each particle, the forces on that particle from other particles are summed.

I.e. the force on particle i, $\mathbf{F}_i$, is given by

$$\mathbf{F}_i = \sum_{j=1}^{n'} \mathbf{F}_{ij}, \tag{2.36}$$

where $\mathbf{F}_{ij}$ is the force on particle i from particle j and the prime on the summation indicates that we exclude $i = j$.

This simple method is prohibitive, because operations scale as N^2 with N particles. Further-more, if the time step of the simulation is such that particles propagate distances comparable to the inter-particle distance in one time step, non-physical forces can result. E.g. if the particles interact via the coulombic interaction, we may have the case where after one time step two particles lye at the same position, leading to an infinite force.

However, in cases where the physics of the system require details of the interactions on very small scales to be resolved, this may be unavoidable, since it directly calculates these forces. In our situation we require to look at this particle-particle scale of the system for collisions, but our calculations only require the interaction between pairs of particles and once particles are paired the are excluded from further calculations.

2.6.1.2 Particle-Mesh Method

To decrease computational intensity of the calculation of forces, one must make approximations which resemble the nature of the force, allowing us to operate with less information. The PM method does this by considering the resultant force field produced by all the particles and approximates this field using a grid (Mesh) of discrete points in space. The forces on particles are then interpolated from this grid. This has the advantage of reducing the scaling of the number of operations required to N plus $N_m^3 \log_2 N_m^3$ for a $N_m \times N_m \times N_m$ mesh [16]. Typically, we deal with situations where $N \sim 10^5$ and $N_m \sim 50$, so for a rough comparison, the PP method requires $\sim N^2 = 10^{10}$ operations, while the PM method requires $\sim N + N_m^3 \log_2 N_m^3 = 10^5 + 50^3 \log_2 50^3 \sim 2 \times 10^6$ per time step. Clearly we wish to be using the PM method over the PP method where possible.

The down side is that with only this grid of values, it cannot resolve force fluctuations well on length scales less than the grid spacing.

We define the space around any one grid point, which is closer to that grid point than any other grid point as the *cell* of that grid point.

2.6.1.3 Particle-Particle-Particle-Mesh Method

The P^3M method is a hybrid of the PP and PM methods. It uses the PP method for forces which vary rapidly on scales small compared to that of the grid spacing and the PM method for slowly varying long ranged forces.

It may be the case that the force which you are concerned with can be split up into a slowly varying component and a rapidly varying component.

This decomposition is essentially what occurred in Section 2.5, where the interactions of the atoms were decomposed into the HF mean field term (approximated by the PM method)

and the collision integrals, which require us to use a variant of the PP method for calculating collisions of particles.

2.6.2 Issues of the Particle-Mesh Method

There are a few issues with the PM method, which have their roots in how the force grid is calculated from the particles and how the forces on particles are interpolated from this grid.

An important issue arises when one uses the nearest grid point (NGP) scheme. This is when the charge[6] attributed to a particle is mapped to the nearest grid point to the particle.

The particle may move anywhere within the cell of the grid point and not have any effect on the calculated force grid. However, if the particle leaves that cell the force changes discontinuously. This of course will be less of a problem when each cell contains a large number of particles, since the addition/removal of a single particle will have a negligible effect on the overall force.

As a manifestation of this problem we note that as we change the grid (e.g. grid spacing or translate it) the calculated force will vary by the discretization.

To reduce these effects it is useful to distribute the charge of particles over more than just the one point. This indeed is an effective approach and has been analysed in great detail in the literature [16, 19]. This results in a hierarchy of assignment schemes; at first order is the NGP scheme. Second order is the so called cloud in a cell (CIC) scheme, which takes into account the position of the particle relative to two grid points. In one-dimension the CIC scheme can be described by the assignment function,

$$W(x) = \begin{cases} \left(1 - \frac{|x|}{H}\right) & -H < x < H \\ 0 & \text{otherwise} \end{cases} \tag{2.37}$$

where H is the cell width and x is the position relative to a grid point. This assignment function give the proportion of the charge allocated to any grid point and the force on the particle from any grid point. Higher order schemes assign values to more grid points, thus, increasing smoothness.

The assignment schemes in the case of our simulations are best view as interpolation schemes for the assignment of density to a grid and the assignment of forces to particles. However, we note they may also be interpreted as setting the particles to have some physical shape with charge uniformly spread across it. The charge allocated to any grid point is then the integral of the proportion of the particle within the grids cell, multiplied by the total charge of the particle. For example, the shape of the particle for the NGP scheme is a delta function, while in CIC the particle takes the form of a top hat function, hence, explaining the choice of name.

[6] We use the term "charge" to indicate the origin of the interaction force between particles. Our atoms are of course neutral and the interaction between them arises from Van der Waals interaction.

Mixed and Unmixed Assignment Schemes

If finite difference methods are employed for calculating gradients required for calculating forces and the same assignment function is used for force generator assignment and force interpolation, one can show ([16]) that momentum is conserved. That is the force between particles is equal and opposite and there is no self force on any particle.

If one was to use different assignment functions, the force between particles will still be equal and opposite, but it is not the case anymore that the self force is zero. E.g. using NGP for charge assignment and CIC for force interpolation leads to exponentially unstable motion!

Chapter 3

Equilibrium Properties of the Classical Boltzmann Equation

We look into this topic because it is required for initialization and analysis of our simulations presented in Chapter 5. Also, we have seen (Section 2.5) that the structure of the quantum Boltzmann equation does not quite agree with the classical Boltzmann equation, due to it having the HF mean field potential. This is not intrinsically a quantum effect, indeed classically one might also expect this as well, because for the case of repulsive interactions, the particles will be repelled away from areas of high density.

Equilibrium is established when the phase-space distribution is time-independent, i.e. the number of particles entering and leaving each phase-space cell are balanced. Under these conditions, we see immediately from Eqs. 2.5 and 2.8 that the equation of motion reduces to the streaming terms,

$$\left(\frac{\partial}{\partial t} + \frac{\mathbf{p}}{m} \cdot \nabla_{\mathbf{r}} - \nabla_{\mathbf{r}} U_{ext}(\mathbf{r}) \cdot \nabla_{\mathbf{p}}\right) f(\mathbf{r}, \mathbf{p}, t) = 0, \tag{3.1}$$

i.e. the collision integral vanishes.

This equation is satisfied if the phase-space distribution can be written as a function of the energy, i.e. $f(H_1)$, where $H_1 = \frac{p^2}{2m} + U_{ext}(\mathbf{r})$ is the Hamiltonian. This tells us that the equilibrium distribution has nothing to do with the particle-particle interactions in the static external potential case. As mentioned earlier this is counter intuitive, but before exploring this further we pause to give the functional form of the equilibrium distribution,

$$f(\mathbf{r}, \mathbf{p}, t) = \aleph \exp\left[-\beta\left(\frac{p^2}{2m} + U(\mathbf{r})\right)\right], \tag{3.2}$$

where $\aleph$ is some normalization factor, where $\beta = \frac{1}{k_B T}$ with T is the temperature of the system and k_B is the Boltzmann constant.

We have chosen to show this result by appealing to H-theorem (see Appendix A), but one could also obtain this result using Boltzmann statistics and saying that the collisions are only a means of redistributing the energy of the system about the particles.

To see why the collisions have no effect on the equilibrium distribution we look at an exact equation of motion for $f(\mathbf{r}, \mathbf{p}, t)$, given by [13]:

$$\left(\frac{\partial}{\partial t} + \frac{\mathbf{p}}{m} \cdot \nabla_{\mathbf{r}} - \nabla_{\mathbf{r}} U_{ext}(\mathbf{r}) \cdot \nabla_{\mathbf{p}}\right) f(\mathbf{r}, \mathbf{p}, t) = \int d^3 r_2 d^3 p_2 \nabla_{\mathbf{r}} V_{int}(\mathbf{r} - \mathbf{r}_2) \cdot \nabla_{\mathbf{p}} f_2(\mathbf{r}, \mathbf{p}, \mathbf{r}_2, \mathbf{p}_2, t). \tag{3.3}$$

We see two new objects; $V_{int}(\mathbf{r}-\mathbf{r}_2)$ is the two-body interaction potential and $f_2(\mathbf{r}, \mathbf{p}, \mathbf{r}_2, \mathbf{p}_2, t)$ is the probability of finding a particle at point $(\mathbf{r}, \mathbf{p})$ and another at $(\mathbf{r}_2, \mathbf{p}_2)$, at time t. In Section 2.3 we assumed this to be $f(\mathbf{r}, \mathbf{p}, t) f(\mathbf{r}, \mathbf{p}_2, t)$, but in general this is not the case (correlations may exist between the particles). We see that the equation of motion for the one-particle density, $f(\mathbf{r}, \mathbf{p}, t)$, depends on the two-particle density, $f_2(\mathbf{r}, \mathbf{p}, \mathbf{r}_2, \mathbf{p}_2, t)$. Therefore, we also need an equation of motion for the two-particle density. However, the equation of motion for the two-particle density depends on the three-particle density and so on. Thus, we have a hierarchy of equations (The Bogoliubov-Born-Green-Kirkwood-Yvon hierarchy (BBGKY)). With various assumptions and physical justifications one can truncate the BBGKY hierarchy and reduce Eq. 3.3 to the Boltzmann equation [13]. However, let us not do this and continue to work with the full Eq. 3.3 for now.

We have seen that the potential which we are concerned with is well approximated by (see Section 2.4)

$$V_{int}(\mathbf{r} - \mathbf{r}_2) \to g\delta(\mathbf{r} - \mathbf{r}_2), \tag{3.4}$$

for low energy collisions. We take this and assume that position and momentum are uncorrelated, as we did for the derivation of the Boltzmann Equation in Chapter 2, i.e. set $f_2(\mathbf{r}, \mathbf{p}, \mathbf{r}_2, \mathbf{p}_2, t) = f(\mathbf{r}, \mathbf{p}, t) f(\mathbf{r}, \mathbf{p}_2, t)$. Then using Eq. 3.4, the right-hand-side of Eq. 3.3 can be evaluated to give,

$$\left(\frac{\partial}{\partial t} + \frac{\mathbf{p}}{m} \cdot \nabla_{\mathbf{r}} - \nabla_{\mathbf{r}} U_{ext}(\mathbf{r}) \cdot \nabla_{\mathbf{p}}\right) f(\mathbf{r}, \mathbf{p}, t) = g \nabla_{\mathbf{r}} n(\mathbf{r}, t) \cdot \nabla_{\mathbf{p}} f(\mathbf{r}, \mathbf{p}, t), \tag{3.5}$$

where $n(\mathbf{r}, t)$ is the density of particles at position $\mathbf{r}$ at some time t.

$$\left(\frac{\partial}{\partial t} + \frac{\mathbf{p}}{m} \cdot \nabla_{\mathbf{r}} - \nabla_{\mathbf{r}} (U_{ext}(\mathbf{r}) + g n(\mathbf{r}, t)) \cdot \nabla_{\mathbf{p}}\right) f(\mathbf{r}, \mathbf{p}, t) = 0. \tag{3.6}$$

We see this has the effect of modifying the potential in the streaming terms by the strength of interaction multiplied by the number of particles at that point, as expected by the nature of the interaction (Eq. 3.4). Eq. 3.6 can be easily simulated via a self-consistent calculation of the density of the particles at each time step of the simulation.

The question is now, why and how we lost this information in the derivation of the Boltzmann equation? Lets define the problem in another form, which makes the answer clear.

Observe at equilibrium we have the following two contrasting equations

$$\left(\frac{\partial}{\partial t} + \frac{\mathbf{p}}{m} \cdot \nabla_{\mathbf{r}} - \nabla_{\mathbf{r}} U_{ext}(\mathbf{r}) \cdot \nabla_{\mathbf{p}}\right) f(\mathbf{r}, \mathbf{p}, t) = 0 \tag{3.7}$$

$$\left(\frac{\partial}{\partial t}+\frac{\mathbf{p}}{m}\cdot\nabla_{\mathbf{r}}-\nabla_{\mathbf{r}}(U_{ext}(\mathbf{r})+gn_0(\mathbf{r}))\cdot\nabla_{\mathbf{p}}\right)f(\mathbf{r},\mathbf{p},t)=0, \tag{3.8}$$

where $n_0(\mathbf{r})$ is the equilibrium density of the cloud. This tells us that the somewhere in the derivation of the Boltzmann equation we have assume that the density of the cloud does not vary over space. This is in fact true, because when integrating over all impact parameters, we made the following statement.

> "Here we are assuming that the effective range of the interaction potential is within d^3r. Otherwise, while we integrate over all impact parameters, we are integrating outside of the volume d^3r. If this was the case, we should be using the expression $f(\mathbf{r}(\Omega),\mathbf{p}_2,t)$ for the phase-space density".

We assumed that the phase-space density was constant over the range of interaction. Thus, removing any possibility for an effective potential including the particle density.

Chapter 4

Numerical Methods

4.1 Implementation of Jackson and Zaremba

As stated earlier, evolution of the condensate is not a primary concern of this project. Indeed, previous research by the Otago group has established an efficient approach, known as the Runge-Kutta 4th order Interaction Picture (RK4IP) method, ([27]) for evolving the Gross-Pitaevskii equation. Here we will be concerned with developing a method for evolving the thermal cloud, closely following the approach of Jackson and Zaremba [11].

The next three subsections detail the three main steps of the method: (i) calculation of thermal cloud density and force, (ii) collisionless evolution of particles, and (iii) particle collisions.

4.1.1 Thermal Cloud Density and Calculation of Forces

The thermal cloud phase-space density, $f(\mathbf{r}, \mathbf{p}, t)$, may be represented by a swarm of test particles, which evolve according to Newton's laws [16]

$$f(\mathbf{r}, \mathbf{p}, t) = \frac{N_p h^3}{N_T} \sum_{i=1}^{N_T} \delta(\mathbf{r} - \mathbf{r}_i(t)) \delta(\mathbf{p} - \mathbf{p}_i(t)), \tag{4.1}$$

where h is Planck's constant, N_p is the number of physical atoms and N_T is the number of test particles, which in general can differ from the number of physical atoms. We see in Chapter 5 that we require $N_T \sim 10^5$ for good statistics. Eq. 4.1 is normalized such that when integrated over all phase-space it gives $N_T h^3$.

The thermal cloud density is required in the HF mean field terms appearing in the equations of motion for the condensate and thermal cloud. However, using this discrete particle description, the thermal cloud density is a collection of delta functions, i.e.

$$n_t(\mathbf{r}, t) = \frac{N_p}{N_T} \sum_{i=1}^{N_T} \delta(\mathbf{r} - \mathbf{r}_i(t)). \tag{4.2}$$

Jackson and Zaremba employed a smoothing scheme, different than that outlined in Section 2.6.2. First the test particles are assigned to a mesh via the CIC scheme and then the resultant mesh is convolved with an isotropic, normalized Gaussian.

In the context of Section 2.6.2, this is interpreted as the test particles taking the physical form of a top hat (CIC) and the interaction potential assume the form of a Gaussian. To decrease computation time, the convolution was performed in Fourier space, taking advantage of the fact that convolution is equivalent to multiplication in Fourier space.

It is noted that the property of zero self force is preserved, since, the gradient of a Gaussian at its centre is identically zero.

The choice of using the CIC scheme to initially smooth the distribution seems redundant, however, it does allow you to have less mesh points. This is because, if we were to simply use the NGP scheme one would find that test particles in the same cell would have zero force on each other. Thus, we cannot have cell sizes which washout small scale fluctuations that would be important to the physics of the problem. The CIC scheme incorporates the positions of the test particles within the cells, allowing for small scale fluctuations to be resolved to some degree. One must remember that the CIC scheme is inherently more computationally intensive and it may be faster to use a denser grid with the NGP scheme.

4.1.2 Collisionless Evolution of the Thermal Cloud

If the typical collision time scale, τ, is such that $\tau \gg \Delta t$, where Δt is the time step of the simulation, then collisions of the particles can be treated separately from the collisionless evolution of the particles. Here we discuss the collisionless evolution of the test particles and in the next section we will deal with the collisions.

Jackson and Zaremba [11] opted to use symplectic integrators instead of Runge-Kutta methods for performing the time evolution. This is because symplectic integrators tend to conserve quantities (e.g. energy) better over long time periods for Hamiltonian systems [17]. However, it is noted that having a variable time step can nullify this property of the symplectic integrators. Symplectic integrators are designed to conserve the symplectic structure of Hamiltonian systems, $d^3r d^3p = d^3r' d^3p'$. They conserve this by enforcing that the leap frog transformations of $\mathbf{r}$ and $\mathbf{p}$ are canonical transformations.

In [11] a second-order symplectic operator was used, which is most elegantly shown by using Lie formalism [17]. The evolution of the phase-space coordinates $\mathbf{z}_i = (\mathbf{p}_i, \mathbf{r}_i)$ is given by the equation

$$\frac{d\mathbf{z}_i}{dt} = \{\mathbf{z}_i, H_i\} \equiv - i\mathcal{L}\mathbf{z}_i, \tag{4.3}$$

where $H_i = \frac{p_i^2}{2m} + U_{ext}(\mathbf{r}_i, t)$ is the single particle Hamiltonian, $\mathcal{L}$ is the Liouville operator, and $\{A, B\}$ corresponds to the Poisson bracket of A and B, i.e.

$$\{A, B\} = \sum_{j=1}^{3N} \left(\frac{\partial A}{\partial r_j} \cdot \frac{\partial B}{\partial p_j} - \frac{\partial A}{\partial p_j} \cdot \frac{\partial B}{\partial r_j} \right) \tag{4.4}$$

The exact solution to Eq. 4.3 is given by

$$\mathbf{z}(t+\Delta t) = \exp(-i\mathcal{L}\Delta t)\mathbf{z}(t) \tag{4.5}$$

If we split the Hamiltonian into kinetic $T(\mathbf{p}_i)$ and potential $U_{ext}(\mathbf{r}_i, t)$ energy terms, we may make use of the Baker-Campbell-Hausdorff formula [18].

$$\exp(A)\exp(B) = \exp(C) \tag{4.6}$$

where

$$C = A + B + \frac{1}{2}[A,B] + \frac{1}{12}([A,[A,B]] + [B,[B,A]]) + \frac{1}{24}[A,[B,[B,A]]] + \ldots \tag{4.7}$$

This gives us

$$\exp(-i\mathcal{L}\Delta t)\mathbf{z} = \exp(-i\mathcal{L}_T\frac{\Delta t}{2})\exp(-i\mathcal{L}_U\Delta t)\exp(-i\mathcal{L}_T\frac{\Delta t}{2}) + O(\Delta t^3), \tag{4.8}$$

also known as a Suzuki-Trotter decomposition.

The second-order symplectic integrator scheme is obtained when we take the first term of Eq. 4.8, which we see is accurate to second-order in Δt. This has the effect of updating the phase-space variables in leap frog fashion

$$\begin{aligned} \mathbf{q}_i &= \mathbf{r}_i(t) + \tfrac{1}{2m}\Delta t\mathbf{p}_i(t) \\ \mathbf{p}(t+\Delta t) &= \mathbf{p}_i(t) - \Delta t\nabla_{\mathbf{r}}U(\mathbf{q}_i, t) \\ \mathbf{r}_i(t+\Delta t) &= \mathbf{q}_i + \tfrac{1}{2m}\Delta t\mathbf{p}_i(t+\Delta t) \end{aligned} \tag{4.9}$$

Jackson and Zaremba found that this second-order symplectic integrator conserved energy in the sense that it oscillates a small amount about some set value, which agrees with our results in Chapter 5.

4.1.3 Particle Collisions

The simulations of this project only concern the collisions between thermal cloud atoms. Thus, we will only develop the method for calculating $C_{22}[f]$ collision integral (Eq. 2.29), understanding that the same principles can be applied to the $C_{12}[f]$ collision integral[1].

The collision integral, $C_{22}[f]$, was approximated by a MC sampling technique that allowed the test particles to be associated with the MC samples. This results in the probability that two test particles (i, j) paired at random (understanding any one of these particles cannot be paired with any of the other test particles), in a cell of volume V_{cell} about the mesh point $\mathbf{r}$, undergo a collision with each other in the time step Δt, is given by

$$P_{ij}^{22}(\mathbf{r}, t) \simeq n_t(\mathbf{r}, t)\frac{|\mathbf{p}_i - \mathbf{p}_j|}{m}\int \frac{d\Omega}{4\pi}\sigma(1+f_3)(1+f_4)\Delta t. \tag{4.10}$$

[1]The details concerning the $C_{12}[f]$ collision integral are found in [11].

The derivation of the probability 4.10 can be viewed in Appendix B. We note that an important realization in this derivation, which is not explained by Jackson and Zaremba [11]. That is, there are two possible choices for the density which links the MC samples to the test particles in the simulation, which describe different situations. The first choice is to use the density of the thermal cloud, which leads to the correct sampling of the collision integral, $C_{22}[f]$. However, it does not correctly describe the dynamics of the test particles. The other is the choice of the test particle density, which results in the correct dynamics and the collision probability Eq. 4.10.

The collision probability Eq. 4.10, allows one to simulate collisions in a manner consistent with the collision integral $C_{22}[f]$. To realize this in the simulation, at each time step the test particles are binned into cells in position space. In each bin the test particles are paired at random and for each pair their momenta are updated if they undergo a collision determined by Eq. 4.10.

To evaluate Eq. 4.10, we also need to know the momentum distribution of the physical atoms in the cell to evaluate the phase-space densities f_3 and f_4. This information is taken from the test particles by binning them onto a momentum space grid with the CIC scheme. The CIC scheme was used to reduce statistical fluctuations.

We know from Section 2.2 that the final momenta of the test particles must lie of a sphere centred at $\frac{1}{2}(\mathbf{p}-\mathbf{p}_2)$ with radius $\frac{|\mathbf{p}_2-\mathbf{p}_1|}{2}$ and the scattering angles θ and ϕ determine the final state. In [11] the final state (Ω_R) was chosen randomly, which then sets the collision probability to be

$$P_{ij}^{22}(\mathbf{r},t) \simeq n_t(\mathbf{r},t)\frac{|\mathbf{p}_i-\mathbf{p}_j|}{m}\sigma(1+f_3^{\Omega_R})(1+f_4^{\Omega_R})\Delta t \tag{4.11}$$

This is valid provided the time step is small, such that, the test particles on average "experience" the correct probability of a collision (Eq. 4.10), before propagating a distance significant to the scale of the system. We discus an alternative procedure for determining the collision probabilities in the next section.

Now that a probability of such a collision has been calculated, the collision goes ahead if $R < P_{ij}^{22}$ where R is a uniformly distributed random variable on the range $[0,1]$.

4.1.4 Discussion of Collision Probability

Typically the integral in Eq. 4.10,

$$P_{ij}^{22}(\mathbf{r},t) \simeq n_t(\mathbf{r},t)\frac{|\mathbf{p}_i-\mathbf{p}_j|}{m}\int\frac{d\Omega}{4\pi}\sigma(1+f_3)(1+f_4)\Delta t, \tag{4.12}$$

is extremely difficult to solve analytically, due to the phase-space density terms, f_3 and f_4. Hence, we are evolving the thermal cloud with these discrete particle methods. Furthermore, we only have a few pieces of information about the densities, f_3 and f_4, which we extract from the test particle distribution in the cell in question. The amount of information increases with increasing test particle number, but so does the computation time.

After calculating the integral in Eq. 4.12, we are still required to select the final states of the pair of test particles, which reflects that states are non-equiprobable, due to the stimulated Bose scattering. As stated in the previous section, Jackson and Zaremba do this by choosing one set of final states and use this to determine the probability of the collision. This requires the values of f_3 and f_4 to be interpolated from the momentum grid for the test particles in this cell.

To achieve a more accurate calculation of the integral, we are required to take more samples of the integral and average the results. With the requirement of an interpolation scheme for f_3 and f_4, this becomes a very computationally intensive problem.

We illustrate in the next section the steps required to perform this calculation and suggest a possible scheme for avoiding the binning of the test particles in momentum space, hence, the interpolation required for determining f_3 and f_4.

4.1.4.1 Outline of Sampling Method

Eq. 4.12 may be approximated by randomly selecting a set of final states lying on the sphere determined by the initial momentum states of the pair of test particles and for each of these final states, Eq. 4.12 is evaluated. Then an approximate solution to Eq. 4.12 is obtained by averaging these results. To randomly select these final states without preference to any direction, one must select uniformly distributed random numbers on the ranges $\cos\theta \in [-1, 1]$ and $\phi \in [0, 2\pi]$. The densities for these final states must be obtained from the momentum space grid of the test particles, employing some interpolation scheme, which is inherently computationally intensive.

In sampling Eq. 4.12 in this manner, we obtain a set of probabilities given by

$$P^{22}_{ijk}(\mathbf{r}, t) \simeq n_t(\mathbf{r}, t)\frac{|\mathbf{p}_i - \mathbf{p}_j|}{m}\sigma(1 + f_3^{\Omega_k})(1 + f_4^{\Omega_k})\Delta t, \tag{4.13}$$

where Ω_k are the angles defining the final state k. Thus, the approximate solution is given by

$$P^{22}_{ij}(\mathbf{r}, t) \simeq n_t(\mathbf{r}, t)\frac{|\mathbf{p}_i - \mathbf{p}_j|}{m}\sigma\Delta t\frac{1}{N_s}\sum_{k=1}^{N_s}(1 + f_3^{\Omega_k})(1 + f_4^{\Omega_k}), \tag{4.14}$$

where N_s is the number of samples.

Remembering that the test particles must scatter into a defined state, we must keep the probability information obtained from the randomly selected samples and use a stacked probability method for determining the outcome of a collision.

Stack probabilities is easiest explained when considering the case study in Fig. 4.1, showing the integral has been sampled eight times. The eight probabilities are stacked on top of each other and are normalized, such that, when summed they result in the probability given by Eq. 4.14. A number is randomly selected $R \in [0, 1]$ and where this random number falls determines the collision outcome. In Fig. 4.1, R fell in the region where the outcome is given by the scattering angles Ω_8. If it was to fall in the region $P^{\Omega}_{ij} = 0$, no collision would go ahead.

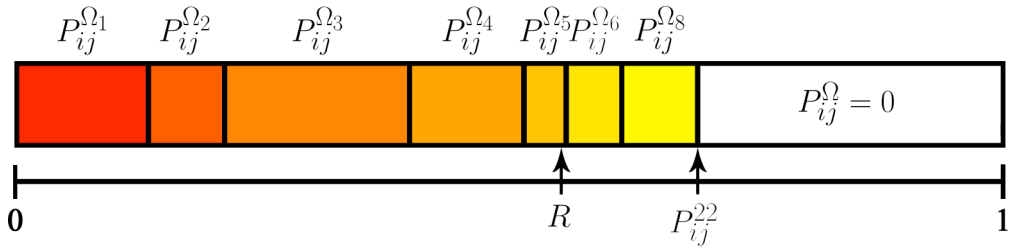

$$P_{ij}^{\Omega_k}(\mathbf{r},t) \simeq \tfrac{1}{N_s}\tilde{n}(\mathbf{r},t)\tfrac{|\mathbf{p}_i-\mathbf{p}_j|}{m}\sigma(1+f_3^{\Omega_k})(1+f_4^{\Omega_k})\Delta t$$

Figure 4.1: Stacked Probabilities.

4.1.4.2 Possible Approximation for Increased Computational Speed

In the previous section, one notices that a large amount of computation is required for binning the test particles in momentum space and the interpolation required for obtaining values for f_3 and f_4. It is possible one can sidestep these requirements by assuming that the momentum of the test particles are locally thermalized in momentum space. With this approximation we may write the following for the momentum distribution $\mathcal{K}^i(p_x,p_y,p_z)$ in the cell i.

$$\mathcal{K}^i(p_x,p_y,p_z) = \frac{N_{cell}}{V_{cell}}\frac{1}{(2\pi)^{\frac{3}{2}}\sqrt{\langle p_x^2\rangle\langle p_y^2\rangle\langle p_z^2\rangle}}\exp\left[-\frac{1}{2}\left(\frac{(p_x-\langle p_x\rangle)^2}{\langle p_x^2\rangle}+\frac{(p_y-\langle p_y\rangle)^2}{\langle p_y^2\rangle}+\frac{(p_z-\langle p_z\rangle)^2}{\langle p_z^2\rangle}\right)\right], \tag{4.15}$$

where $\langle\rangle$ refers to the average of the test particles in cell i. With the knowledge

$$\begin{aligned}\mathbf{p}_3 &= \left(P_x+\tfrac{|\mathbf{u}|}{2}\sin\theta\cos\phi, P_y+\tfrac{|\mathbf{u}|}{2}\sin\theta\sin\phi, P_z+\tfrac{|\mathbf{u}|}{2}\cos\theta\right)\\ \mathbf{p}_4 &= \left(P_x-\tfrac{|\mathbf{u}|}{2}\sin\theta\cos\phi, P_y-\tfrac{|\mathbf{u}|}{2}\sin\theta\sin\phi, P_z-\tfrac{|\mathbf{u}|}{2}\cos\theta\right)\end{aligned} \tag{4.16}$$

where

$$\begin{aligned}\mathbf{P} &= \tfrac{1}{2}(\mathbf{p}_1+\mathbf{p}_2)\\ \mathbf{u} &= \mathbf{p}_2-\mathbf{p}_1\end{aligned} \tag{4.17}$$

The Eqs. 4.15, 4.16 and 4.17, give us continuous equations for f_3 and f_4. Only requiring various averages of the momenta of the test particles, we have avoided binning test particles in momentum space and interpolation. Furthermore, this allows for the possibility of increasing the time step of the simulation, since we no longer require the probability (given by Eq. 4.12) to be sampled in time. However, we still need the time step to be small enough such that $P_{ij}^{22} < 1$. Otherwise, during the collisionless evolution of the test particles, it may be the case they have propagated in the wrong direction for a significant amount of time, when they should have earlier had a collision.

This approximation of local thermal equilibrium must be tested to determine if it is a physically credible assumption, which is left for future research. However, it is expected that is most applicable in near equilibrium situations.

4.2 Details of Our Implementation

Here we outline outline briefly the numerical method we used. As we have discussed many aspects in the previous section, we will only expand on the areas which have not been detailed in the previous section.

4.2.1 Equations of Motion

As an initial step to understanding the the implementation of Jackson and Zaremba, the stimulated Bose scattering and mean field terms were ignored. This means the probability of a pair to suffer a collision (Eq. 4.10) integrates to

$$P_{ij}^{22}(\mathbf{r},t) \simeq n_t(\mathbf{r},t)\frac{|\mathbf{p}_i - \mathbf{p}_j|}{m}\sigma\Delta t. \tag{4.18}$$

This is the equivalent to assuming we have classical particles governed by the Boltzmann equation, with total differential cross-section equal to that of the total bosonic cross-section, $\sigma = 8\pi a^2$.

The choice of momentum as a variable is not convenient for simulations. What proves to be more effective is the choice of using wave vectors, which are related to momentum by the de Broglie relation, $\mathbf{p} = \hbar\mathbf{k}$.

Rewriting Eqs. 4.9 and for $\mathbf{k}$ and dropping all condensate interactions, we have

$$\begin{array}{c} \mathbf{q}_i = \mathbf{r}_i(t_n) + \frac{\hbar}{2m}\Delta t\mathbf{k}_i(t_n) \\ \mathbf{k}(t+\Delta t) = \mathbf{k}_i(t) - \hbar\Delta t\nabla_{\mathbf{r}}U(\mathbf{q}_i,t) \\ \mathbf{r}_i(t+\Delta t) = \mathbf{q}_i + \frac{\hbar}{2m}\Delta t\mathbf{k}_i(t+\Delta t) \end{array} \tag{4.19}$$

$$P_{ij}^{22}(\mathbf{r},t) \simeq n_t(\mathbf{r},t)\frac{\hbar\,|\mathbf{k}_i - \mathbf{k}_j|}{m}\sigma\Delta t \tag{4.20}$$

where $U(\mathbf{r},t) = U_{ext}(\mathbf{r}) + 2g\tilde{n}(\mathbf{r},t)$. In the cases presented in Chapter 5, the external potential take the form of a isotropic harmonic trap, $U_{ext}(\mathbf{r}) = \frac{\omega^2}{2}(x^2+y^2+z^2)$, with trapping frequency ω.

4.2.2 Computational Units

It is desirable to make a good choice of units to make all relevant equations dimensionless. A convenient choice of units for length and time are, respectively,

$$x_0 = \sqrt{\tfrac{\hbar}{2m\omega}} \qquad\qquad t_0 = \tfrac{1}{\omega} \tag{4.21}$$

Other units of interest may be derived from these choices. E. g., the unit of energy

$$\epsilon_0 = \frac{\hbar\omega}{2} \tag{4.22}$$

Dimensionless quantities are denoted with a tilde, e.g. position $\widetilde{\mathbf{r}} = \frac{\mathbf{r}}{x_0}$.

4.2.2.1 Dimensionless Equations

The equations we require for propagating the thermal cloud in our simulation take the dimensionless form

$$\begin{aligned} \widetilde{\mathbf{q}}_i &= \widetilde{\mathbf{r}}_i(\widetilde{t}) + \Delta\widetilde{t}\,\widetilde{\mathbf{k}}_i(t) \\ \widetilde{\mathbf{k}}(\widetilde{t}+\Delta\widetilde{t}) &= \widetilde{\mathbf{k}}_i(\widetilde{t}) - \tfrac{\Delta\widetilde{t}}{2}\left(\widetilde{\mathbf{q}}_i + 2\widetilde{g}\,\nabla_{\widetilde{\mathbf{r}}}\,\widetilde{n}_t(\widetilde{\mathbf{q}}_i,\widetilde{t})\right) \\ \widetilde{\mathbf{r}}_i(\widetilde{t}+\Delta\widetilde{t}) &= \widetilde{\mathbf{q}}_i + \Delta\widetilde{t}\,\widetilde{\mathbf{k}}_i(\widetilde{t}+\Delta\widetilde{t}) \end{aligned} \tag{4.23}$$

$$\widetilde{P}_{ij}^{22} = 2\widetilde{n}_t(\widetilde{\mathbf{r}}_i,\widetilde{t})\widetilde{\sigma}\Delta\widetilde{t}\left|\widetilde{\mathbf{k}}_i - \widetilde{\mathbf{k}}_j\right| \tag{4.24}$$

Here we have explicitly shown the gradient of the potential in Eqs. 4.19. Although $\widetilde{P}_{ij}^{22}$ was already dimensionless (it is a probability), we have denoted it with the tilde to avoid confusion.

The classical equilibrium phase-space distribution takes the dimensionless form

$$f(\widetilde{\mathbf{k}},\widetilde{\mathbf{r}}) = N_p\left(\frac{\widetilde{\beta}}{\pi}\right)^3 \exp\left[-\widetilde{\beta}\left(2\left(\widetilde{k}_x^2+\widetilde{k}_y^2+\widetilde{k}_z^2\right)+\frac{1}{2}\left(\widetilde{x}^2+\widetilde{y}^2+\widetilde{z}^2\right)\right)\right] \tag{4.25}$$

This phase-space distribution is normalized to the total number of physical atoms of the system.

4.2.3 Algorithm

There are two distinct procedures required at each time step to implement Eqs. 4.23 and 4.24. Streaming of the test particles and calculations of collisions.

The below we briefly outline these procedures:

4.2.3.1 Streaming

Streaming consists of implementing the Eqs. 4.23,

$$\begin{aligned} \widetilde{\mathbf{q}}_i &= \widetilde{\mathbf{r}}_i(\widetilde{t}) + \Delta\widetilde{t}\,\widetilde{\mathbf{k}}_i(t) \\ \widetilde{\mathbf{k}}(\widetilde{t}+\Delta\widetilde{t}) &= \widetilde{\mathbf{k}}_i(\widetilde{t}) - \tfrac{\Delta\widetilde{t}}{2}\left(\widetilde{\mathbf{q}}_i + 2\widetilde{g}\,\nabla_{\widetilde{\mathbf{r}}}\,\widetilde{n}_t(\widetilde{\mathbf{q}}_i,\widetilde{t})\right) \\ \widetilde{\mathbf{r}}_i(\widetilde{t}+\Delta\widetilde{t}) &= \widetilde{\mathbf{q}}_i + \Delta\widetilde{t}\,\widetilde{\mathbf{k}}_i(\widetilde{t}+\Delta\widetilde{t}) \end{aligned} \tag{4.26}$$

The first and last of these equations are simple to implement, since they only require the addition of matrices. In the cases we present in Chapter 5, we do not consider the mean field term appearing in the second term. Thus, this term also reduces to a simple addition of the positions of the particles to the wave vectors.

However, if we were to introduce the mean field term several steps in the calculation would arise. First, the particles would have to be binned onto a density grid. As mentioned earlier, Jackson and Zaremba use the CIC scheme to do this, but test would have to be performed to determine if there is merit in using this scheme. As it adds more computation time than the NGP scheme, due to the extra degree of interpolation.

This distribution would have to be smoothed by convolving it with a Gaussian. This would be done in Fourier space taking advantage of convolve in multiplication in Fourier space, since it is much faster to perform the convolution this way. Again, further tests would have to be undertaken to determine the effects of changing the width of the Gaussian.

We would take the derivative of this distribution in Fourier space, because of the enhanced accuracy of taking derivatives in this manner, opposed to finite difference method.

Finally, the distribution is returned to position space and the force on particles has to be interpolated with some scheme from the resultant grid.

4.2.3.2 Collisions

When binning the test particles one wants to represent the distribution of the test particles accurately. Thus, the bin distribution must reflect the structure of the problem, i.e. more bins are required where the distribution changes rapidly. Since, we consider non-equilibrium cases (see Chapter 5) our binning procedure is adaptive in the sense it senses where the distribution changes most rapidly and distributes the bins accordingly. I.e. more bins are distributed over the regions were the distribution changes most rapidly.

We chose a coordinate system such that our initial conditions have some symmetry with respect to our $\widetilde{x}$, $\widetilde{y}$, and $\widetilde{z}$ axes. This allows us to use rectangular bins distributed on a cartesian grid to describe the distribution. This distribution is illustrated in Fig. 4.2. We see than an artifact of this distribution is the heavily binned region $\mathcal{R}$. In Chapter 5, the results of Section 5.1 force us to simulate in a regime where this region is not an issue. However, it is noted, because one wishing to perform these simulations must keep it mind as it may cause problems to manifest.

After binning of the test particles, each bin is considered individually and pairs of particles are randomly determined, understanding that particles can only be paired with one other particle.

The collisions of those pairs are determined in a fashion similar to that of Section 4.1.4. However, with being able to analytically evaluate the integral in equation 4.10, we no longer need to select a set of possible outcomes of the collision. We need only determine a collision occurs and then select a random final state for the test particles to scatter into.

This happens to be the most time consuming component of each time step (typically 80-90% of the total time). However, it is noted that the collision calculation for each bin is independent of any other bin. Thus, the speed can be hugely increases by employing parallel, since the calculations of each bin are independent you can pass different processor different sets of bins.

4.2.4 Sampling Initial Conditions

The initial conditions of the test particles where determined using a simple MC acceptance and rejection scheme, which we outline for a simplified 1D example below.

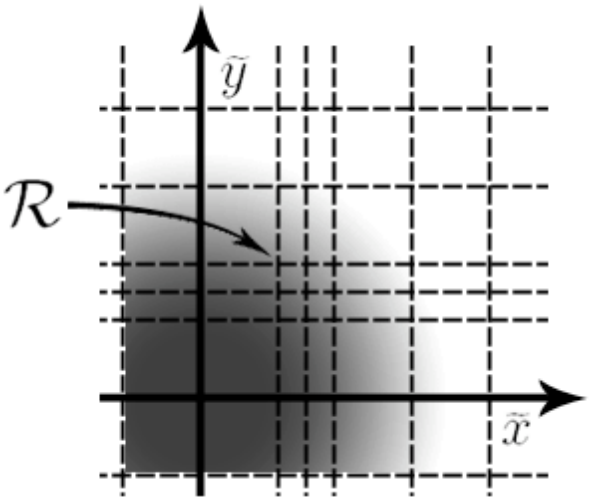

Figure 4.2: Bin Distribution: The dashed lines show the boundaries on the bins, understanding that these dash lines generalize to all quadrants of position space. The shaded region indicates a possible density distribution of atoms, which is heavily binned in the region indicated by $\mathcal{R}$.

Say the initial distribution of $\widetilde{k}_x$ and $\widetilde{x}$ was given by,

$$\mathcal{D}(\widetilde{k}_x, \widetilde{x}) = N_p \frac{\widetilde{\beta}}{\pi} \exp\left[-\widetilde{\beta}\left(2\widetilde{k}_x^2 + \frac{\widetilde{x}^2}{2}\right)\right]. \tag{4.27}$$

The algorithm goes as follows:

Select random numbers for the particle coordinates of the desired distribution (in our case $\widetilde{k}_x^R$ and $\widetilde{x}^R$) on the range where the distribution is non-zero. For distributions like the one considered, it may be non-zero everywhere (except $\pm\infty$), so some reasonable choice for the range must be made over which the vast majority of particles are contained.

Now select an random number, R, in the range $[0, \mathcal{D}_{max}]$, where $\mathcal{D}_{max}$ is the maximum value of the distribution (in our case $\mathcal{D}_{max} = N_p \frac{\widetilde{\beta}}{\pi}$). If $R \leq \mathcal{D}(\widetilde{k}_x^R, \widetilde{x}^R)$, then the values of $\widetilde{k}_x^R$ and $\widetilde{x}^R$ are accepted as the wave vector and position of a test particle.

The process is repeated until the required number of of test particles are generated. This collection of test particles then constitutes a sampling of the distribution 4.27.

Chapter 5

Results

Various dynamical simulations were undertaken as tests of the method and implementation, and to characterize its performance. We have chosen a few case studies to present in this section, which are important tests and/or are rich with interesting physics. These results will help showcase what our algorithm is capable of simulating.

5.1 Monte Carlo Collision Rates

Here we test the mean collision rate calculated by the MC collision scheme against that of the theoretical mean collision rate. We find that the discretization of the phase-space density, $f(\widetilde{\mathbf{k}}, \widetilde{\mathbf{r}}, \widetilde{t})$, both with the finite number of test particles and a spatial grid, leads to difficulties associated with the discretization that need to be carefully monitored. In particular we show that one must choose the optimum number of spatial bins for a chosen number of test particles.

As mentioned in Appendix B, if we use the density of the thermal cloud for linking the MC samples to the test particles, we obtain the mean collision rate of the thermal cloud atoms. Thus, for the purposes of this test, we use the probability for a pair to collide corresponding to this choice, i.e. the physical particle collision rate is given by

$$\widetilde{P}_{ij}^{22} = 2\frac{N_p}{N_T}\widetilde{n}_t(\widetilde{\mathbf{r}}, \widetilde{t})\widetilde{\sigma}\Delta\widetilde{t}\left|\widetilde{\mathbf{k}}_i - \widetilde{\mathbf{k}}_j\right|. \tag{5.1}$$

Using Eqs. 4.25, B.4, and B.5, we obtain the dimensionless equation for the mean collision rate along the $\widetilde{x}$ axis,

$$\widetilde{R}_0^{22}(\widetilde{x}) = N_p^2\frac{\sqrt{2}}{8}\widetilde{\sigma}\,\widetilde{v}_{th}\left(\frac{\widetilde{\beta}}{\pi}\right)^2 \exp\left[-\widetilde{\beta}\,\widetilde{x}^{\,2}\right]. \tag{5.2}$$

From Eq. B.11, it is clear that the corresponding rate from the MC simulation is given by

$$\widetilde{R}_0^{22}(\widetilde{x}, \widetilde{t}_n) \simeq 2\sum_{(ij)}\frac{\widetilde{P}_{ij}^{22}(\widetilde{x}, \widetilde{t}_n)}{\widetilde{V}_{cell}\Delta\widetilde{t}}, \tag{5.3}$$

where $\widetilde{t}_n$ indicates the time step n.

Since our simulation consists of discrete test particles, each time step fluctuates and to minimize this we time average Eq. 5.3 over M time steps, giving,

$$\widetilde{R}_0^{22}(\widetilde{x}) = \frac{1}{M}\sum_{n=1}^{M} \widetilde{R}_0^{22}(\widetilde{x}, \widetilde{t}_n). \tag{5.4}$$

The comparison of Eqs. 5.3 and 5.4 can by seen in Fig. 5.1 for a cloud of 5×10^4 physical atoms modelled by 2×10^5 test particles with equilibrium initial condition and $M = 100$. As indicated we show this for the cases of grids with 32, 48, 64, and 96 bins along each direction.

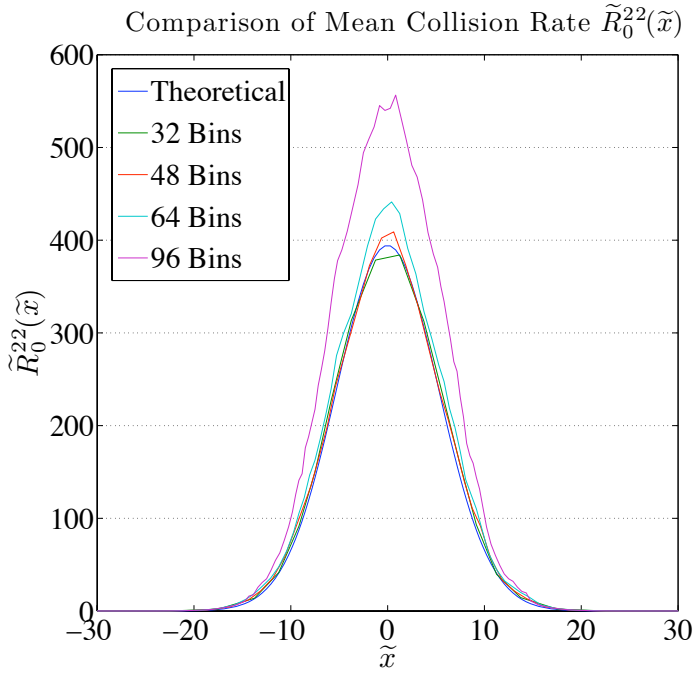

Figure 5.1: Mean Collision Rates Calculated by the MC scheme compared to that of the theoretical prediction for the case of 5×10^4 physical atoms modelled by 2×10^5 test particles. The results are for a selection of bin numbers as indicated by the legend.

We see for increasing number of bins, the mean collision rate calculated by the MC scheme increases. In observing the probability for pairs of test particles to collide (Eq. 5.1) we notice that there are only two possible sources for this increase in collision rate to arise. (i) The density "seen" by the MC scheme and (ii) the relative wavenumbers of the colliding test particles. What we mean by the density "seen" by the MC scheme, is that the MC scheme only considers bins with more than one test particles within, since a single test particle cannot be paired for a collision.

We expect the density to decrease, because we decrease the volumes of the bins by increasing the number of bins. Thus, more and more bins with only a single particle form. This would then decrease the mean collision rate (Eq. 5.3) two-fold, as it decreases the number of

pairs as well as the density appearing in Eq. 5.1. Yet, we still see an overall increase in the mean collision rate. Thus, the decrease in density is over compensated in the mean relative wavenumber of the colliding particles.

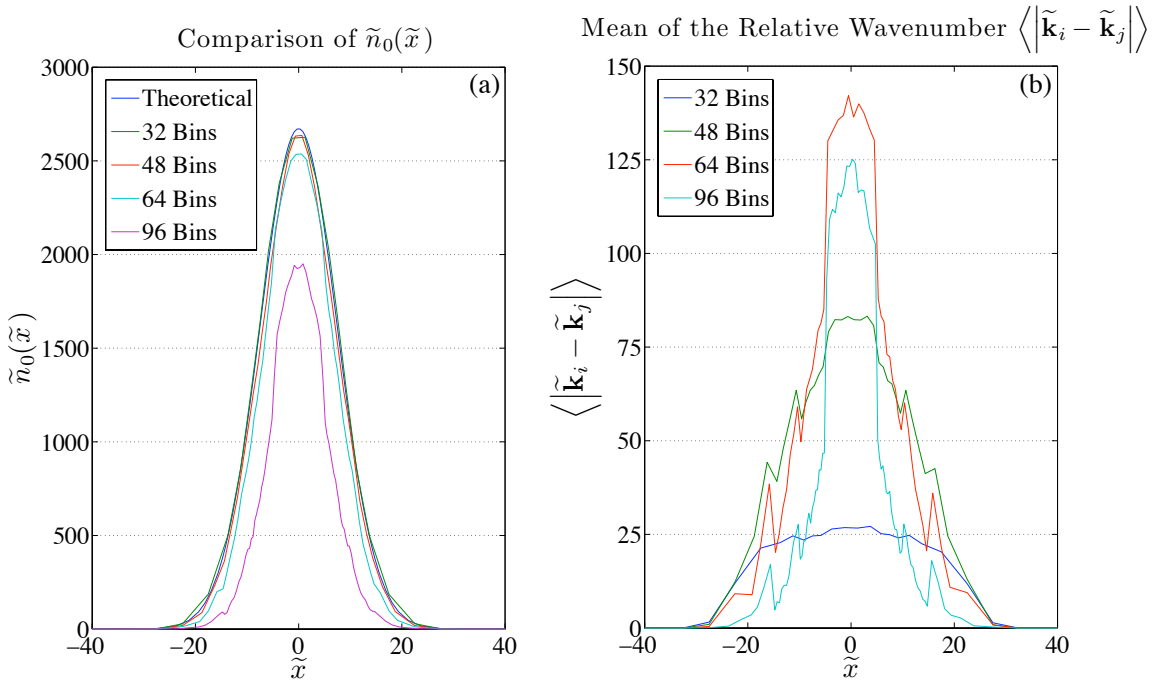

Figure 5.2: The density (a) and mean relative wavenumber (b) calculated by the MC scheme for the bin numbers as indicated by the legends. The density (a) is compared to that of the theoretical prediction.

The results in Figs. 5.2(a) and 5.2(b), show that indeed this is the case. It is seen in Fig. 5.2(b) that the high bin numbers begin to resolve the bin structure. Along with the increase of the mean collision rate, this artifact also effects the dynamics of the simulation. However, we have observed that this effects is reduced with increasing the number of test particles. So we now turn to understand the optimal choice of discretization.

Typically, one wishes to operate in the regime were less than 5% of the test particles are excluded from the MC collisions, which is indicated in Fig. 5.3. We see a decline in the rate at which test particles become excluded with increasing number of bins. This is because, most of the low density regions have been excluded and when we add more bins, the bins are also distributed over these regions.

5.2 Observation of Stable Equilibrium

Here we observe the simulation hold equilibrium for equilibrium initial conditions. This case is an important test of the code and allows us to discuss a variety of phenomena, without the confusion of non-equilibrium dynamics.

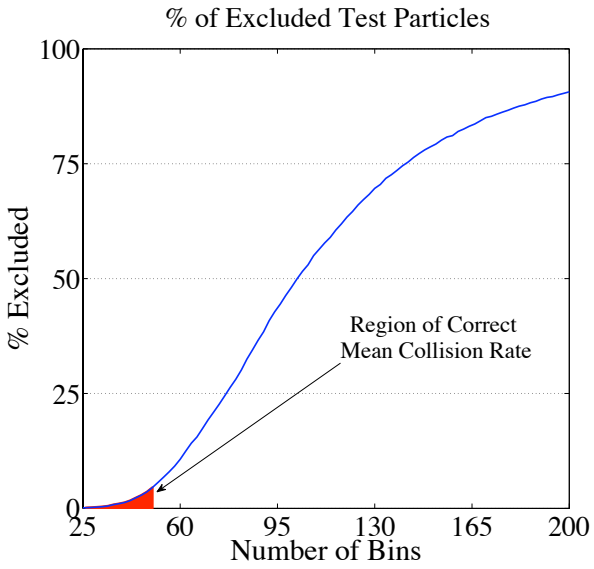

Figure 5.3: The number of bins dependence of the percentage of excluded test particles in the simulation for the case of 2×10^5 test particles. The red region indicated the regime which one would typically wish to simulated in. This graph was obtained by averaging over ten scans of the bin numbers shown.

The presented case is for 5×10^4 physical atoms modelled by 25×10^3, 10^5, and 5×10^5 test particles. The number of bins for each test particle case were optimized in accordance with the test of Section 5.1.

In Figs. 5.4(a) and 5.4(b), we show a comparison of theoretical equilibrium densities in position space

$$\widetilde{n}_0(\widetilde{x}) = N_p \sqrt{\frac{\widetilde{\beta}}{2\pi}} \exp\left[-\frac{\widetilde{\beta}\,\widetilde{x}^2}{2}\right] \tag{5.5}$$

and wave vector space

$$\widetilde{\mathcal{K}}_0(\widetilde{k}_x) = N_p \sqrt{\frac{2\widetilde{\beta}}{\pi}} \exp\left[-2\widetilde{\beta}\,\widetilde{k}_x^2\right], \tag{5.6}$$

to that of which is calculated by the simulation using 5×10^5 test particles at the time $t = 20t_0$ (17ms). We have chosen not to time average the densities calculated by the simulation, as to indicate that instantaneously the simulations distributions describe the physical systems for high numbers of test particle, since, statistical fluctuations fall as $1/\sqrt{N_T}$.

More generally, for cases where the number of particles is less than $N_T \sim 10^5$, statistical fluctuations appear more noticeable and time averaging may be needed for accurate comparisons (E.g. see Figs. 5.5).

We only show the standard deviations of the the $\widetilde{k}_x$ and $\widetilde{x}$ components ($\sigma_{Std}(\widetilde{k}_x)$ and $\sigma_{Std}(\widetilde{x})$) of the test particles in Figs 5.4(c) and 5.4(d), because the standard deviations of the other components show very similar behaviour. The small width oscillation seen at twice the

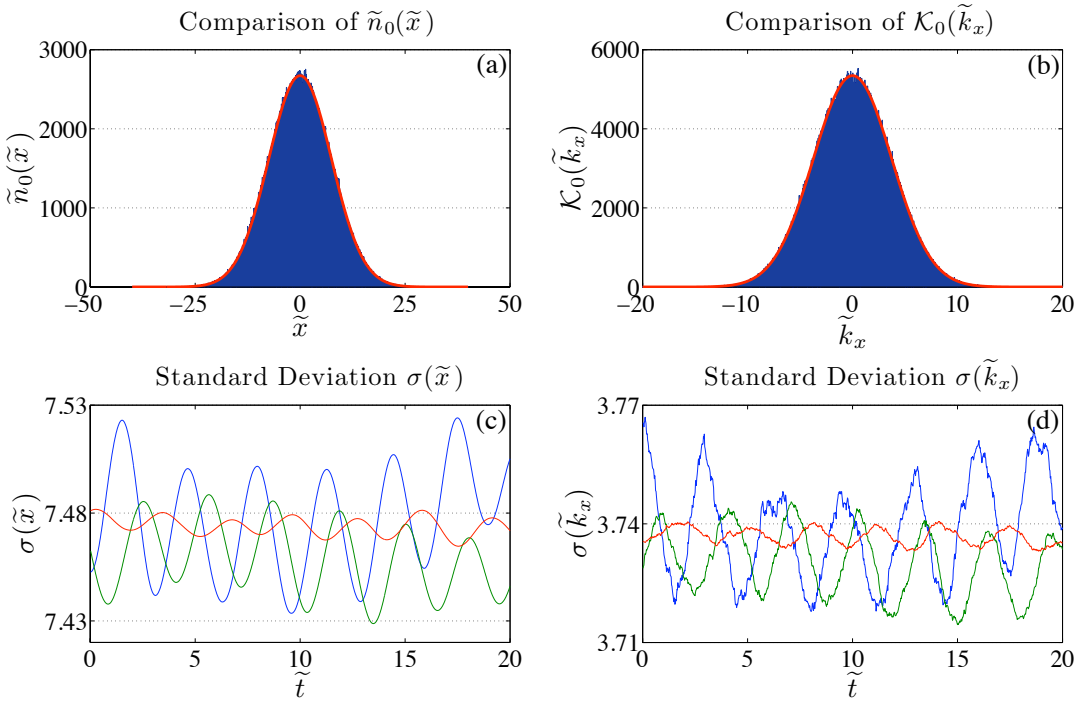

Figure 5.4: The distributions $\widetilde{n}_0(\widetilde{x})$ (a) and $\widetilde{\mathcal{K}}_0(\widetilde{k}_x)$ (b) calculated by the simulation compared to the theoretical prediction (red solid lines). The corresponding standard deviations of $\widetilde{x}$ (c) and $\widetilde{k}_x$ (d) for the cases of 25×10^3 (blue lines), 1×10^5 (green lines), and 5×10^5 (red lines) test particles.

trap frequency arises from the monopole oscillation of the cloud. As the classical system of an isotropic harmonic trap described by the Boltzmann equation, the monopole mode does not damp without the addition of mean field effects [20](we look at a case where we excite this oscillation in Section 5.3). The lack of periodicity in $\sigma_{Std}(\widetilde{x})$ is likely due to the presence of some quadupolar mode (which can damp) and statistical fluctuations, which are more noticeable in the cases with smaller numbers of test particles. However, the jaggedness of Fig. 5.4(d) is due to the random collision processes rearranging the wave vectors.

Apart from this tiny oscillation we can see that overall the position and momentum space, widths are constant in time to the ˜1% level.

We see in Fig. 5.6 that the centre of mass motion of the cloud undergoes harmonic oscillations at the trap frequency. This reflects that any particle-particle interaction, satisfying Newton's third law, has no effect on the centre of mass motion. The property that the centre of mass motion in a harmonic trap is independent of particle-particle interaction and is an undamped mode of oscillation, is a generalized version of Kohn's theorem [21, 22], and is usually referred to as the Kohn mode. The monopole and Kohn mode all arise from asymmetries in the initial conditions and should disappear as $N_T \to \infty$.

Fig. 5.7(a) shows the normalized total number of collisions, i.e. the total number of collisions for each case has been divided by the total number of test particles. The fact that

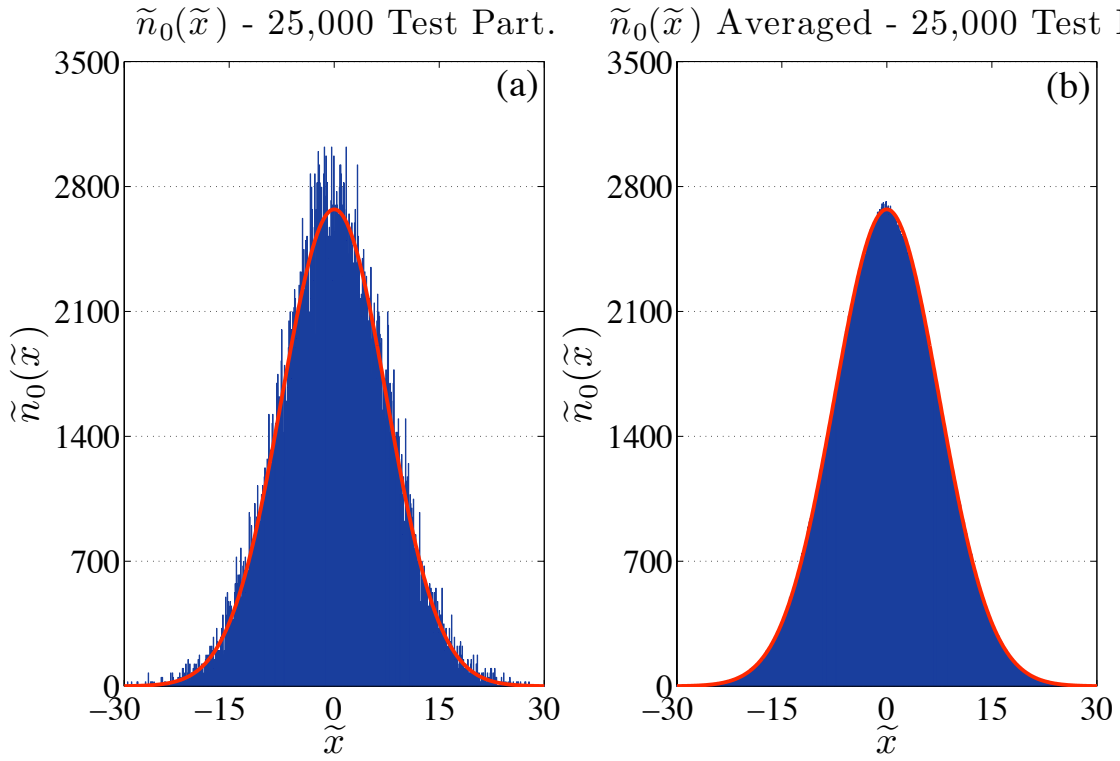

Figure 5.5: The distribution of $\widetilde{x}$ components, $\widetilde{n}_0(\widetilde{x})$, calculated by the simulation compared against the theoretical prediction (red solid lines). (a) shows the distribution at $t = 20t_0$ (17ms), while (b) is averaged over the time interval $t = 12t_0$ (10.2ms).

the plots are close to lying on top of each other give us confidence in the choices of bin numbers and the constant gradient is consistent with the system being in equilibrium.

We see from Fig. 5.7(b) that the energy is conserved in the sense that it oscillates about some value with a very small relative amplitude, which is in agreement with the observations of Jackson and Zaremba [11]. This oscillation is attributed solely to the second-order symplectic integrator used. This was confirmed by observing that the code conserved energy and momentum when streaming was turned off and only the collisions were calculated (the collisions are elastic), and energy varied when simulating the collisionless evolution of the cloud. Fig. 5.7 also shows by decreasing the time step, we decrease the amplitude of oscillation. This is expected for any integrator scheme, as higher order terms in $\triangle\widetilde{t}$ are suppressed.

5.3 Monopole Mode Excitation

As mentioned in the previous section, it has been shown [20] that the monopole mode in an isotropic harmonic trap does not damp in the absence of mean field interactions. As a test of code, we perform a simulation similar to that performed by Bezett and Blakie [4] using the c-field method. We use initial conditions for an excited form of the quadrupolar mode

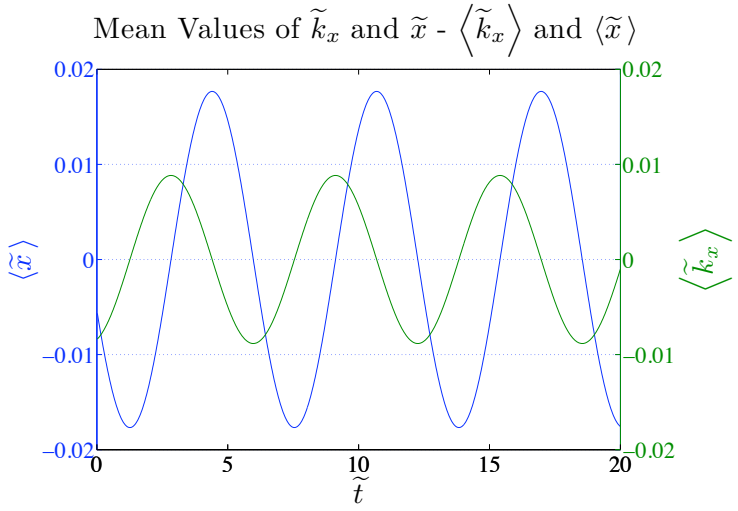

Figure 5.6: Mean values of the $\widetilde{k}_x$ and $\widetilde{x}$ components of the test particles. This indicates the centre of mass motion of the cloud undergoes simple harmonic motion.

$m = 0$, which soon after damps, giving way to a monopole mode.

The initial conditions are for the equilibrium distribution of a harmonic trap with trapping frequencies,

$$\omega_x^2 = \tfrac{3}{4}\omega_0^2 \qquad \omega_y^2 = \omega_0^2 \qquad \omega_z^2 = \omega_0^2 \ . \tag{5.7}$$

I.e. the sampled distribution is of the form

$$S(\mathbf{r}, \mathbf{k}, t) = \aleph \exp -\widetilde{\beta} \left(2 \left(\widetilde{k}_x^2 + \widetilde{k}_y^2 + \widetilde{k}_z^2 \right) + \frac{1}{2} \left(\frac{3}{4}\widetilde{x}^2 + \widetilde{y}^2 + \widetilde{z}^2 \right) \right), \tag{5.8}$$

where $\aleph$ is some normalization factor.

We determine the final equilibrium state for this system by appealing to the equipartition theorem. This relates the total energy to the temperature of the system by,

$$\widetilde{E}_T = \frac{f}{2} N_T \frac{k_B T}{\epsilon_0}, \tag{5.9}$$

where f is the number of degrees of freedom and $\widetilde{E}_T$ is the total dimensionless energy. Eq. 5.9 allows us to readily determine the equilibrium distribution using Eq. 4.25 and $\widetilde{\beta} = \frac{\epsilon_0}{k_B T}$. For the initial conditions determined by Eq. 5.8, the new value is $\widetilde{\beta}_{new} = 0.017$.

For purposes of illustration we chose to simulate 2×10^6 physical atoms, as the quadrupolar mode damps quickly, we can observe a stable monopole mode for an extended period of time. The main results of this section, are presented for the case of 10^6 test particles, which is excessive, but we use it as a benchmark for simulations with less test particles.

The figures of Fig. 5.8 give the standard deviations of all six phase-space variables of the test particles. We see the initial state of the $m = 0$ quadrupolar mode, as the oscillations

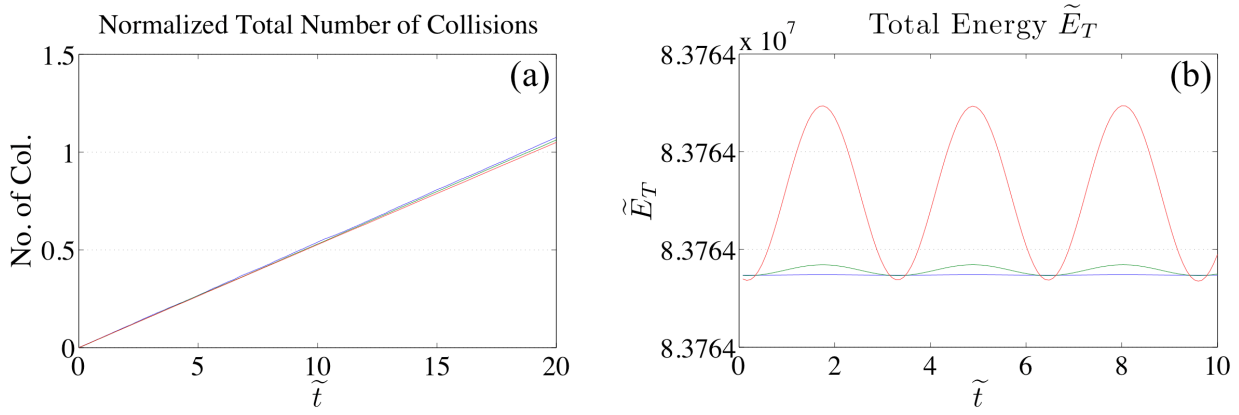

Figure 5.7: (a) shows the normalized total number of collisions for the cases of 25×10^3 (blue line), 10^5 (green line), and 5×10^5 (red line). (b) shows the total energy of the system oscillating with a small amplitude for the cases of $\Delta\widetilde{t} = 0.0005$ (blue line), 0.002 (green line), and 0.008 (red line).

of $\sigma_{Std}(\widetilde{x}\,)$ are initially out of phase by π with that of $\sigma_{Std}(\widetilde{y})$ and $\sigma_{Std}(\widetilde{z})$. This quickly damps giving way to the regular monopole oscillation at twice the trap frequency, where the oscillations of $\sigma_{Std}(\widetilde{x}\,)$, $\sigma_{Std}(\widetilde{y})$, and $\sigma_{Std}(\widetilde{z})$ become in phase. Thus, we find agreement with the results of [20].

Since the energy stored in the degrees of freedom along $\widetilde{x}$ is greater than the other direction, the particles extend into the higher energy regions of the trap along the $\widetilde{x}$ direction. This energy then redistributes itself about all the phase space variables in that all the standard deviations of the other variables increase, while $\sigma_{Std}(\widetilde{x}\,)$ decreases.

While looking at the standard deviations of the phase-space variables, one may wish to ask how many test particles are required to effectively describe the dynamics of this system.

Figs. 5.9(a) and 5.9(b) show the case of 10^5 test particles has good agreement with the benchmark of 10^6. While Figs. 5.9(c) and 5.9(d) show that for the case of 10^4 test particles the monopole oscillation amplitude fluctuates, indicating we have entered a regime that does not describe the correct dynamics of the system. This is just re-iterating the assessment in the previous that we require $N_T \sim 10^5$ for good agreement (small statistical fluctuations) and here we see that small numbers of test particles can directly effect the simulated dynamics

As indicated by Figs. 5.9(a) and 5.9(b), we have chosen the correct density for linking the test particles to the MC samples (See Appendix B). As for the test particle numbers which describe the dynamics of the system correctly, we see that all cases have standard deviation graphs which essentially lie on top of each other within statistical fluctuations. However, we see what is believed to be an artifact of the binning procedure of the wings of the spatial distribution appear in Figs. 5.9(a) and 5.9(c), as an initial bump at the beginning of the graphs. However, further investigation is required to conclude what is causing this.

If we were to choose that density which correctly samples the collision integral (i.e. we used the collision probability in Section 5.1) at any point in time, we would have the dynamics

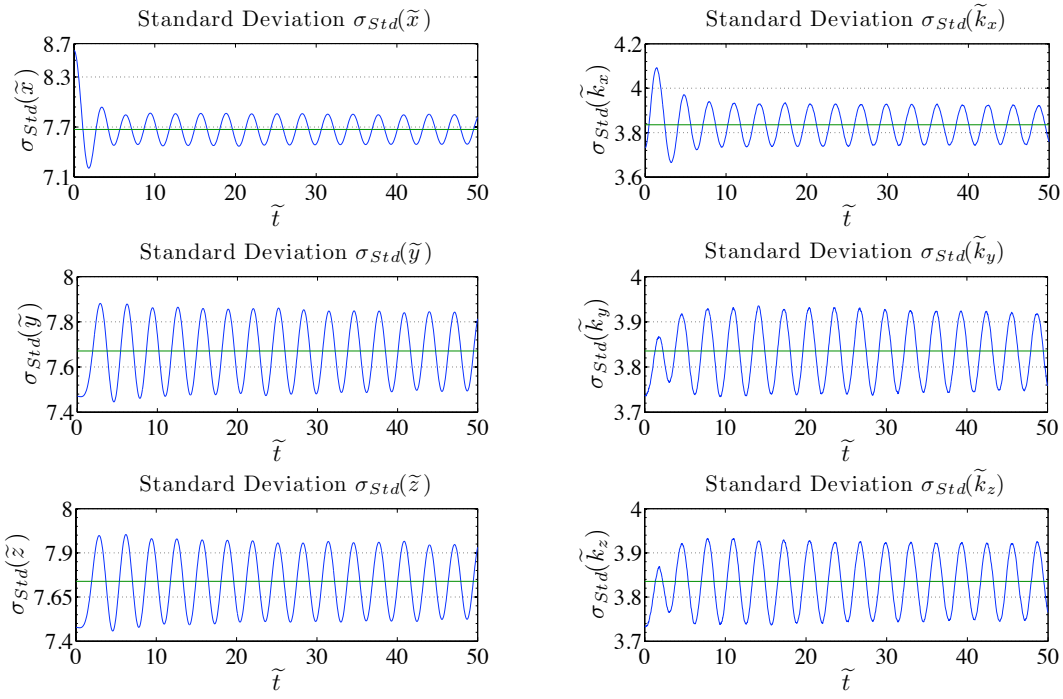

Figure 5.8: Standard Deviations of the phase space variables for 10^6 test particles showing the quadrupolar mode damping, while an excited monopole mode persists. The green lines are the equilibrium standard deviations calculated by the equipartition theorem.

of the system dependent upon the number of test particles in the system. This is observed in Fig .5.10, which shows $\sigma_{Std}(\widetilde{y})$ for the above simulation repeated with this choice of density. We see that each choice of test particle number results in a different dampening rate of the quadrupole mode. This is because each case is enforced to undergo the same amount of collisions. The number of collisions relative to the number of test particles decreases with increasing test particles. Meaning that for the higher test particles cases it is harder for the system to redistribute the initial conditions of the test particles, as this is spread over more test particles, but there are fewer collisions.

For completeness we show the distributions $\widetilde{n}_0(\widetilde{x}\,)$ and $\widetilde{\mathcal{K}}_0(\widetilde{k}_x)$ (Eqs. 5.5 and 5.6) calculated from the simulation against the theoretical, Figs. 5.11. The distributions obtained from the simulation where averaged over three full monopole oscillations to remove statistical fluctuations. We see very good agreement as the maximum differences of both graphs are less than 1%.

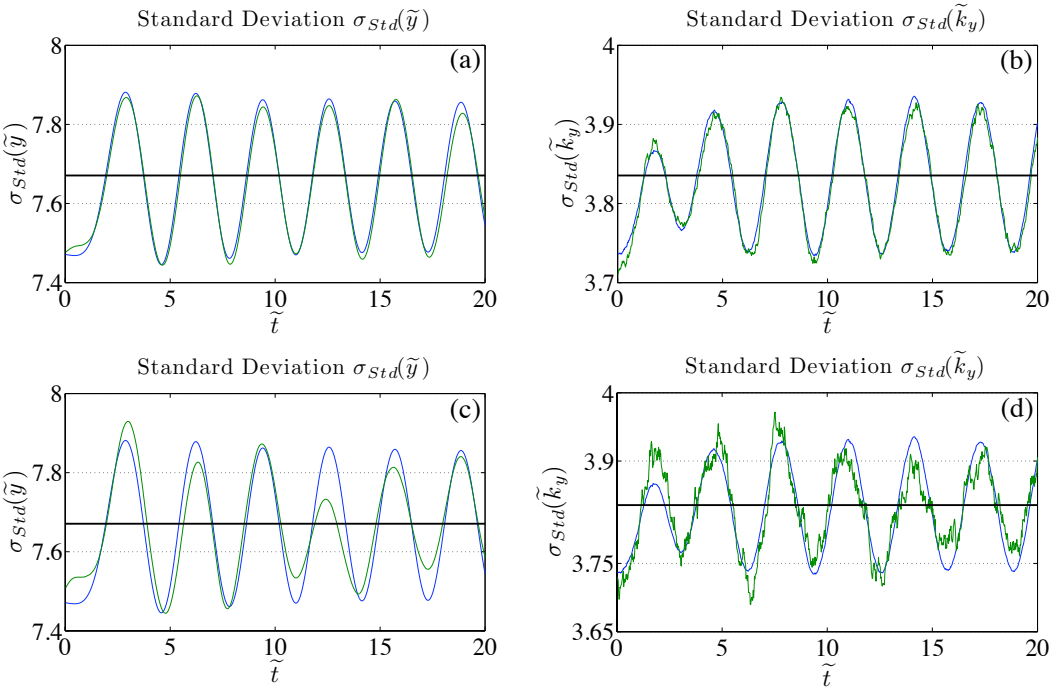

Figure 5.9: The comparison of the standard deviations for $\widetilde{k}_y$ and $\widetilde{y}$ for simulations of 10^5 (a, b) and 10^4 (c, d) test particles against the case of 10^6 test particles (blue line). The black lines indicated the equilibrium standard deviation calculated by the equipartition theorem.

5.4 Collisions of Gaussian Clouds

5.4.1 Free Space Collision of Identical Gaussian Clouds

Here we perform simulations in which we collide two Gaussian clouds of equal mass (i.e. same numbers of physical atoms) in free space. The simulation is performed in the centre of mass frame such that the clouds have equal momentum towards the centre. As explained in Section 2.2, two atoms in the centre of mass frame collide to the spherical shell of possible momenta. Thus, with the collision of the two clouds we expect to see this shell develop in wave vector space, since momentum is related to the wave vector by $\mathbf{p} = \hbar\mathbf{k}$.

The differential cross-section is constant (i.e. s-wave collisions) for all scattering angles, we expect this shell to by filled uniformly. Also, the shell will have some finite width, as the two Gaussian clouds have a finite width in their wave vector distributions.

The quantum degenerate case of colliding BECs has been performed both in experiment [28] and simulation [25] and has a much narrower wave vector distribution, hence well-defined scattering shell. Experiments at Otago have considered a case more similar to what we simulate [23, 24], in which two non-condensed thermal clouds collide.

At $t = 0$, the clouds are set approaching each other ($\widetilde{k}_x = \pm 10$) from offset initial positions

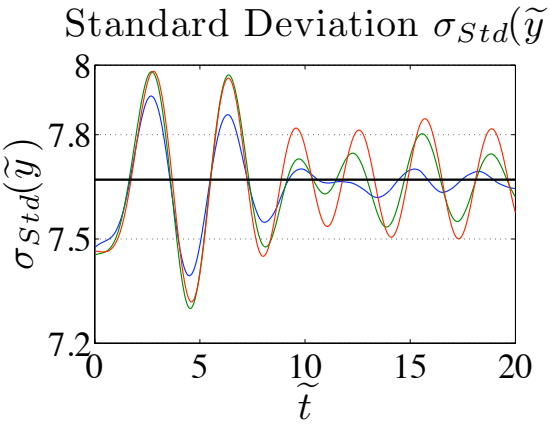

Figure 5.10: Standard deviations of the $\widetilde{y}$ components of the test particles for the case of incorrect collision probabilities. Shows the cases of 10^5 (blue), 2×10^5 (green), and 5×10^5 (red) test particles. The black line is the equilibrium standard deviation calculated by the equipartition theorem.

($\widetilde{x} = \mp 10$). This corresponds to this initial condition

$$f(\widetilde{\mathbf{k}}, \widetilde{\mathbf{r}}, \widetilde{t}) = N_p \frac{\widetilde{\beta}}{\pi} \exp\left[-\widetilde{\beta}\left(2\left|\widetilde{\mathbf{k}} \pm 10\hat{\mathbf{k}}_x\right|^2 + \frac{|\widetilde{\mathbf{r}} \mp 10\hat{\mathbf{x}}|^2}{2}\right)\right], \tag{5.10}$$

that we sample, where $\hat{\mathbf{k}}_x$ and $\hat{\mathbf{x}}$ are unit vectors in the $\widetilde{\mathbf{k}}_x$ and $\widetilde{\mathbf{x}}$ directions, respectively.

In this case we choose $\widetilde{\beta} = 0.07$ and each cloud contains 10^6 physical atoms, which are modelled by a total of 5×10^5 test particles. Figs. 5.12 illustrate projections of the distributions of position and wave vector on to the $\widetilde{x}$ - $\widetilde{y}$ and $\widetilde{k}_x$ - $\widetilde{k}_y$ planes, respectively. Figs. 5.12(a) shows the initial conditions of the system and we see the Gaussian clouds overlap slightly in position space. As indicated by Fig. 5.13(a), the merging of the Gaussian clouds seen in Figs. 5.12(b) is the beginning of the bulk of the collision, since the number of collisions of the test particles begins increasing at a faster rate. We begin to see the faint outline of a halo corresponding to the shell of wave vectors. As it is difficult to see the halo, we have include Fig. 5.13(b), which shows a slice of the $\widetilde{k}_y$ - $\widetilde{k}_z$ plane showing the halo more clearly.

In Figs. 5.12(c), the Gaussian clouds now fully over-lap in position space. The test particles in the shell have undergone second collisions, which deplete the shell to some extent.

Finally, Fig. 5.13(a) shows us at $t = 3.4t_0$ the collision is essentially over, as the number of collisions occurring is greatly reduced. The corresponding position and momentum projection for this time (Figs. 5.12(d)), show a circle of particles centred on $\widetilde{x} = \widetilde{y} = 0$. These particles correspond to the particles in the shell of wave vectors propagating out from the epicentre of the collision in all directions. The remainders of the initial Gaussian clouds continue to propagate in opposite directions, as this case is not dense enough to cause more collisions which would deplete the $\widetilde{k}_x \pm 10$ Gaussian reservoirs.

We demonstrate a situation of this depletion in the following section with an example of a Gaussian cloud collision at higher wavenumbers in a harmonic trap.

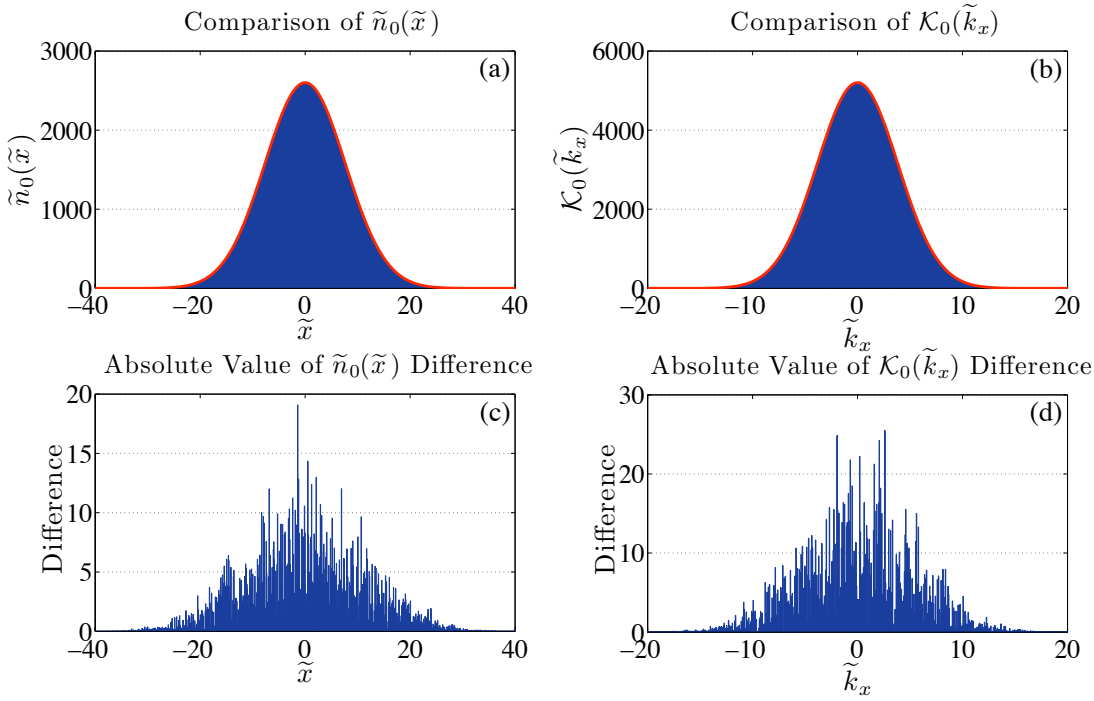

Figure 5.11: The distributions $\widetilde{n}_0(\widetilde{x})$ (a) and $\widetilde{\mathcal{K}}_0(\widetilde{k}_x)$ (b) calculated by the simulation compared to the theoretical prediction (red solid lines). These distributions are averaged over three full monopole oscillations. (a) and (b) are the corresponding absolute values of the difference between the theoretical prediction and simulation.

5.4.2 Collision of Identical Gaussian Clouds in a Harmonic Trap

Here we perform the same simulation as above in a harmonic trap, except now we use two Gaussian clouds positioned at $\widetilde{k}_x \pm 10$ and $\widetilde{x} = \mp 20$ with 25×10^4 physical atoms in each cloud. This a situation where the clouds recollide and are able to thermalize, due to the harmonic trap.

Figs. 5.14(a,b) show us similar behaviour to the free space case, but now the Gaussian distributions in wave vector space move out to greater values, since the particles accelerate down the harmonic potential towards the centre where the two clouds collide. In this case the Gaussians in wave vector space reach out to a maximum of $\widetilde{k}_x = \pm\sqrt{200}$.

When the two clouds become completely overlap, we see the position space distribution in Figs. 5.14(c) begins to deform. Due to the large average relative wave vectors of the two clouds, test particles undergo more collisions than in the free space example in the previous section, redistributing their wave vectors about $\widetilde{k}_x = \widetilde{k}_y = \widetilde{k}_z = 0$ (net wave vector is zero). They find it harder to escape the dense cloud at the centre, since with more collisions they realign their wave vectors more often, tending to travel less distance than what they would without subsequent collisions.

The Figs. 5.15 are a continuation of Figs. 5.14. The first of which (Figs. 5.15(a)) shows the end of this initial collision of the Gaussian clouds. We still have an appreciable number

of uncollided particles with the initial distribution of wave vectors, indicated by the two peaks along the $\widetilde{x}$ axis. However, the majority of the test particles have scattered to form the equilibrium distribution of the system, indicated by the large density situated about $\widetilde{x} = \widetilde{y} = 0$.

There after the clouds recollide (due to the trap) and more closely approach the equilibrium distribution. However significant energy gets trapped in the monopole oscillation which does not thermalize. Figs. (b, c) show the half oscillation of the monopole oscillation, where we have and exchange of energy between the position variables and wave vector variables.

5.5 Future Research

The next steps of this project would be to complete the full classical description of the thermal cloud system. That is, include the meanfield term in the effective potential for the test particles. This well require much more analysis as indicated in Chapter 4. In particular, merits of the CIC scheme for binning the particles and interpolating forces, will have to be weighed against the ease and speed of the NGP method. Also the effects of smoothing the distribution will have to be analysed.

Finally, completing the ZNG description of the thermal cloud without the condensate, we would add in the Bose enhancement terms to the collision integral, $C_{22}[f]$. This requires a significant amount of work, because the calculation of collisions becomes much more computationally intensive and the approximations of Jackson and Zaremba (outlined in Chapter 4) would have to be analysed before any confident predictions can be made with this implementation. The Bose stimulated scattering is a major computational hindrance (see Chapter 4), however the local equilibrium scheme we proposed may be widely applicable to near equilibrium situations and will significantly speed up calculations.

Unlike the ZNG theory, in the c-field approach we only describe the higher energy (lowly occupied) modes with a Boltzmann approach. Hence, it may be feasibly to neglect Bose enhanced scattering for those modes. A major challenge will be to implement a energy cutoff, however, we should be able to do this with a locally varying minimum momentum.

Amongst these future research project, one would want to implement this code in the language C. As this allows one to utilise the power of parallel processor, which we have discussed could easily be applied to the collision calculations, since the collisions of any one bin is independent of all others. This would drastically reduce the computation time of the problem, since currently this calculation attributes to 80-90% of the computation time.

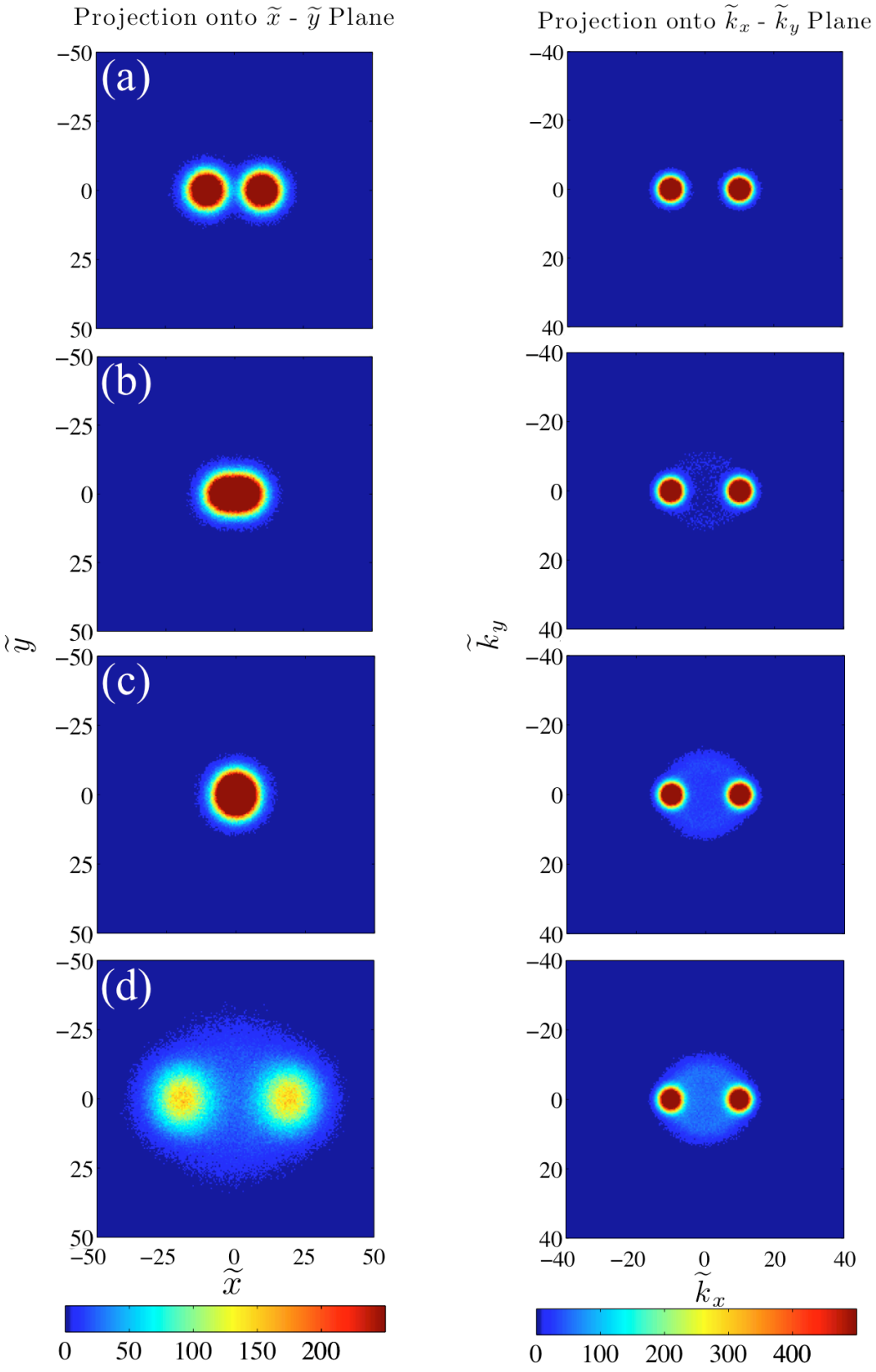

Figure 5.12: Progression of the free space collision of the two Guassian clouds. These are the projects onto the $\widetilde{x}$ - $\widetilde{y}$ and $\widetilde{k}_x$ - $\widetilde{k}_y$ planes for the times $t = 0$ (a), $0.63t_0$ (b), $2t_0$ (c), and $3.4t_0$ (d) (0ms, 0.53ms, 1.7ms, and 2.9ms).

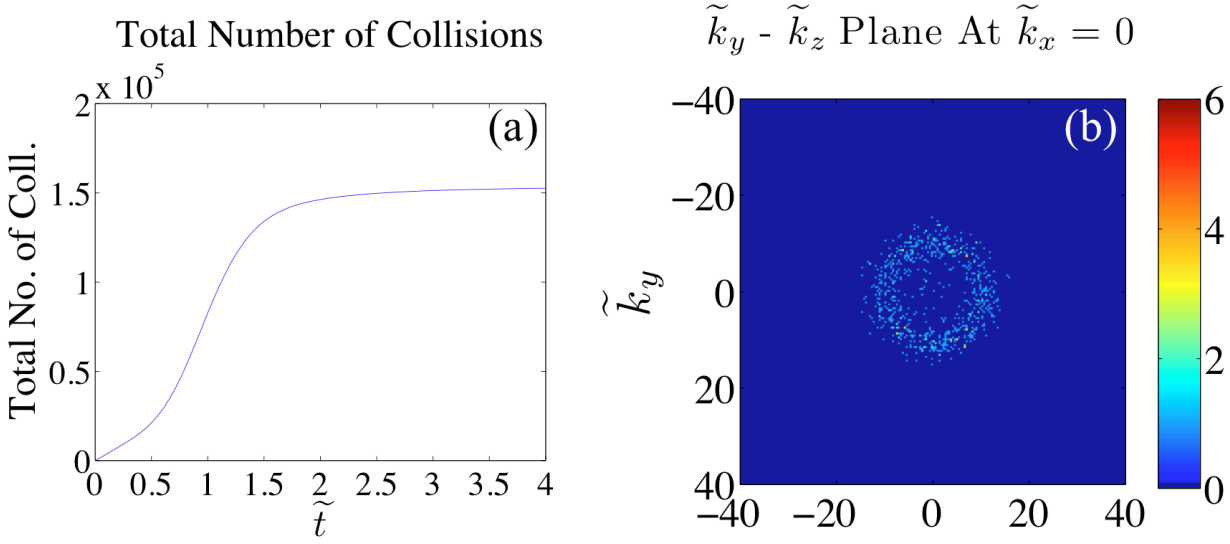

Figure 5.13: (a) shows the total number of collisions of the test particles as the collision progresses. (b) shows a slice of the $\widetilde{k}_y$ - $\widetilde{k}_z$ plane at $\widetilde{k}_x = 0$ demonstrating the halo of wave vectors at $t = 0.63t_0$.

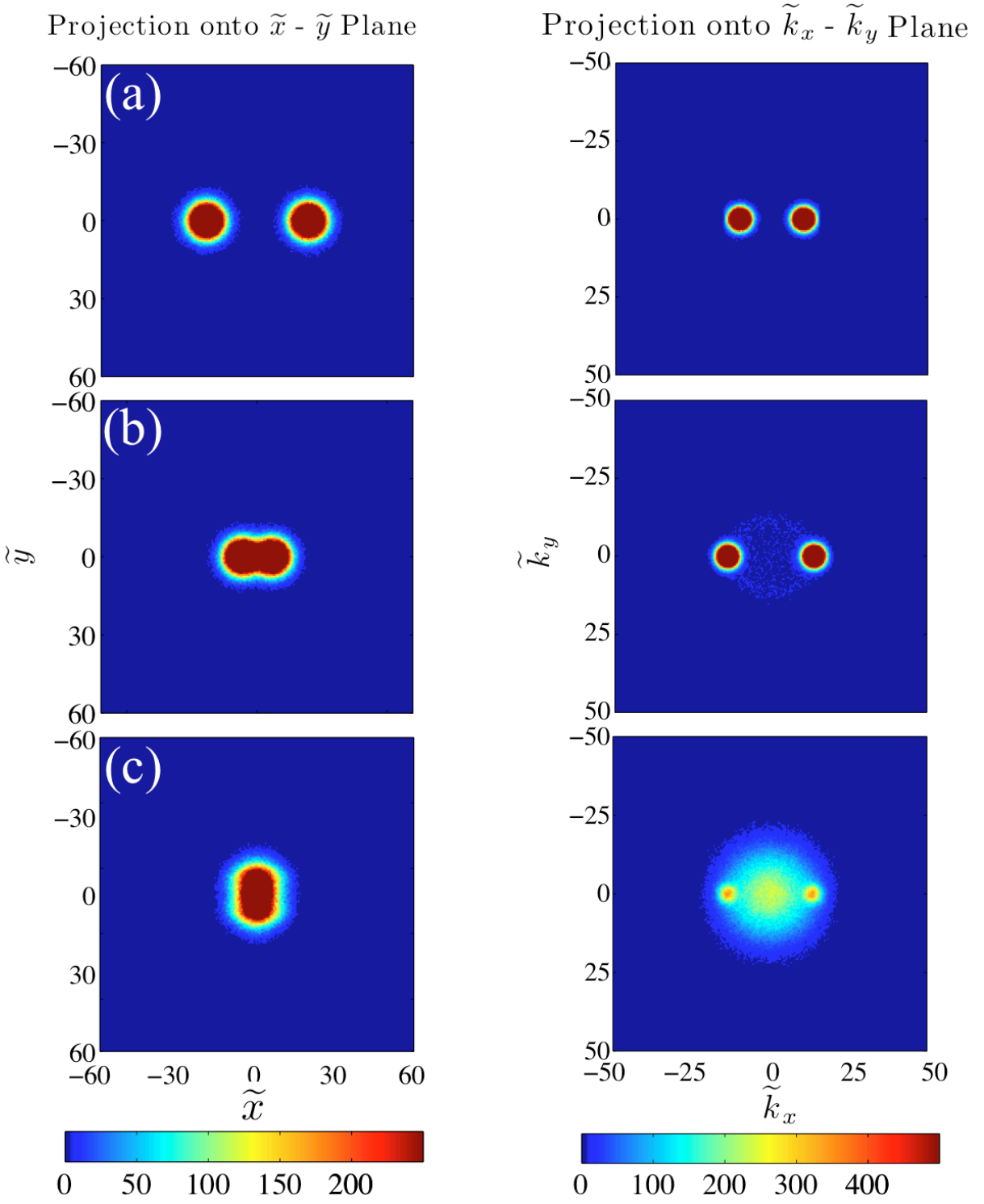

Figure 5.14: Progression of the harmonic trap collision of the two Guassian clouds. These are the projects onto the $\widetilde{x}$ - $\widetilde{y}$ and $\widetilde{k}_x$ - $\widetilde{k}_y$ planes for the times $t = 0$ (a), $0.58t_0$ (b), and t_0 (c) (0ms, 0.49ms, and 0.85ms).

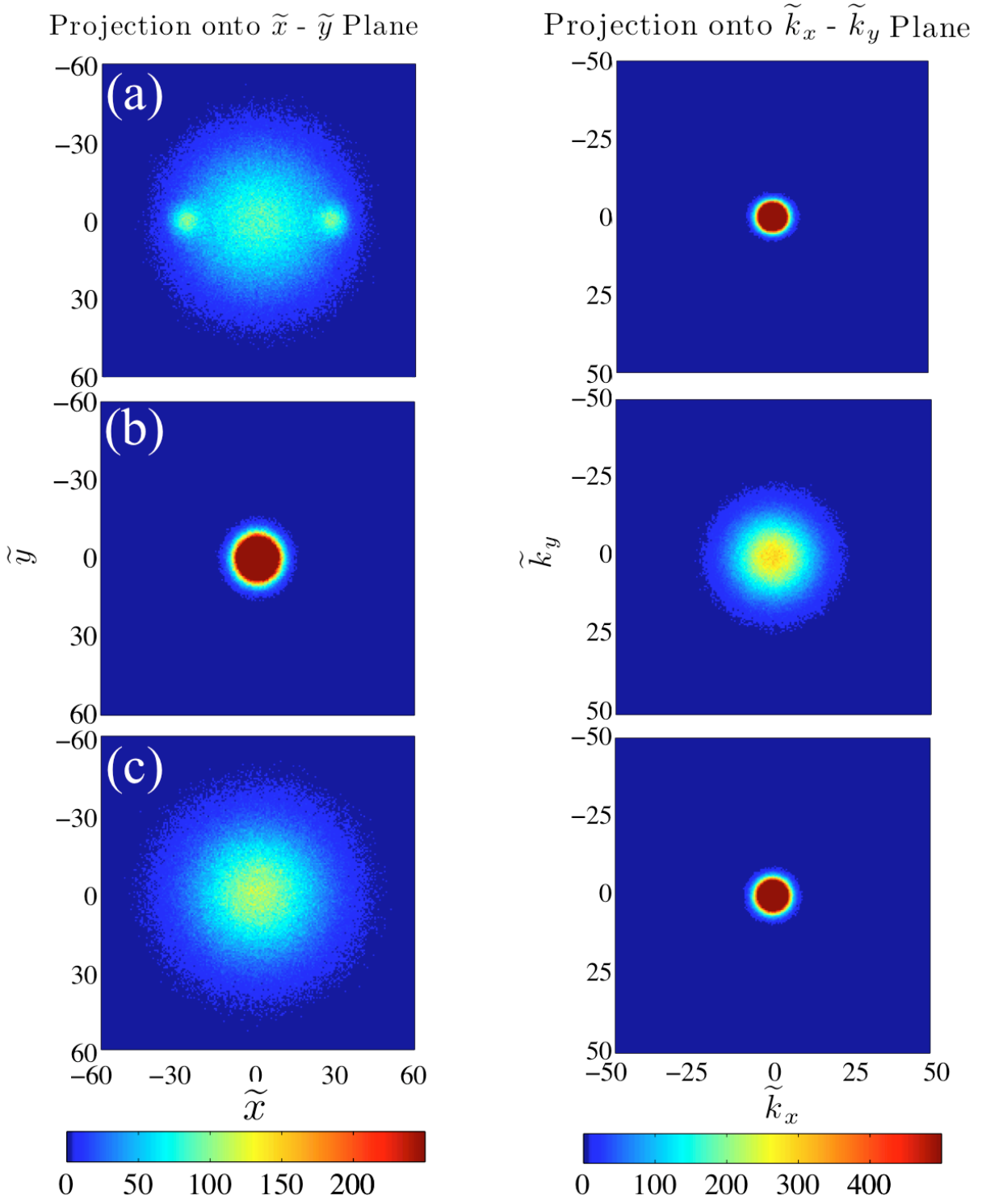

Figure 5.15: Progression of the free space collision of the two Guassian clouds. These are the projects onto the $\widetilde{x}$ - $\widetilde{y}$ and $\widetilde{k}_x$ - $\widetilde{k}_y$ planes for the times $t = 2.2t_0$ (a), $13.48t_0$ (b), and $14.7t_0$ (c) (1.87ms, 11.5ms, and 12.5ms). These Figs. are a continuation of the Figs. 5.14.

Chapter 6

Conclusion

We have conducted a literature review of the derivation of the Boltzmann equation, ZNG formalism, and the particle/MC methods used to solve the quantum Boltzmann equation. This literature review enabled us to explore the inner workings of the methods used by Jackson and Zaremba to simulate the dynamics of the thermal cloud. Along the way various questions have occurred where the literature has not explained details of the theory and implementation. Hence, we have taken the time to answer these questions in full. With this work and expanding on the details of this method, we have built the background required to assimilate this method into c-field theory for a full dynamical description of the thermal cloud. Since, the initial simulations performed by Jackson required super computer resources, we have also suggested possible areas where one can increase the efficiency of the method.

We have successfully implemented these techniques by developing a Boltzmann equation solver, which has undergone various tests showing convergence and agreement with theory. Using this solver, we have demonstrated its ability simulate highly non-equilibrium cases allowing one to study exciting situations. Our code is relatively efficient, being able to simulate $\sim 10^5$ particles for $\sim$ 10ms in 3hours on a desktop computer. The algorithm is intrinsically parallel and future work will be to make a much faster implementation in a complied language using parallelism.

Our suggestions for an efficient local equilibrium scheme will probably led to a fast code that is suitable for simulating close to equilibrium cases, e.g. collective modes.

Appendix A

H-theorem[1]

The H-theorem is a celebrated and also controversial theorem which Boltzmann introduced in 1872. It proves for a system governed by the Boltzmann equation (Eq. 2.20) irreversibly evolves to an equilibrium state. Before the assumptions used to truncate the BBGKY hierarchy, the equations of motion showed no reason for the system to evolve to an equilibrium state, because they are satisfied when considering the reverse trajectory. However, we now know that the processes which lead to equilibrium are themselves reversible, but the equilibrium state is the most probable macroscopic state to be observed [14].

Defining the function $H(t)$ as,

$$H(t) = \int d^3r \int d^3p f(\mathbf{r}, \mathbf{p}, t) \ln f(\mathbf{r}, \mathbf{p}, t) \tag{A.1}$$

The function $H(t)$ is related to the information content of the system and if this is shown to decrease in time, we cannot return to the previous state, because we have lost the information of where the system was. The H-theorem shows that this is the case by obtaining the following equation, in which the integrand is aways positive.

$$\begin{aligned}\frac{dH(t)}{dt} = -\frac{1}{4}\int d^3r \int d^3p \int d^3p_2 \int d\Omega \frac{|\mathbf{p}_2 - \mathbf{p}|}{m}\sigma(\Omega)\times \\ [f(\mathbf{r}, \mathbf{p}, t)f(\mathbf{r}, \mathbf{p}_2, t) - f(\mathbf{r}, \mathbf{p}_1', t)f(\mathbf{r}, \mathbf{p}_2', t)] \times \\ [\ln\left(f(\mathbf{r}, \mathbf{p}, t)f(\mathbf{r}, \mathbf{p}_2, t) - f(\mathbf{r}, \mathbf{p}_1', t)f(\mathbf{r}, \mathbf{p}_2', t)\right)]\end{aligned} \tag{A.2}$$

Furthermore, entropy for a system may be defined as,

$$S(t) = -k_B H(t) \tag{A.3}$$

where k_B is the Boltzmann constant.

We can find the equilibrium phase-space distribution, by knowing at equilibrium $\frac{dH(t)}{dt} = 0$. Since the integrand in Eq. A.2 is always non-zero, this can only occur when $f(\mathbf{r}, \mathbf{p}, t)f(\mathbf{r}, \mathbf{p}_2, t) - f(\mathbf{r}, \mathbf{p}_1', t)f(\mathbf{r}, \mathbf{p}_2', t) = 0$ for all points in space. I.e. for any any two initial momentum vectors

[1] For a detailed discussion of H-theorem refer to pages 71-78 of [13].

$\mathbf{p}_1$ and $\mathbf{p}_2$, every reverse collision has equal probability, so there is no net transfer of momentum. Casting this expression in a new form, by taking the natural log, we have a statement of conservation of momentum.

$$\ln f(\mathbf{r}, \mathbf{p}, t) + \ln f(\mathbf{r}, \mathbf{p}_2, t) = \ln f(\mathbf{r}, \mathbf{p}_1', t) + \ln f(\mathbf{r}, \mathbf{p}_2', t) \tag{A.4}$$

To understand how this is a statement of conservation of momentum, we have to be careful in what we actually mean by Eq. A.4. Remembering that the value $f(\mathbf{r}, \mathbf{p}, t)$ is actually the value of the number of particles in the phase-space volume $d^3r d^3p$ about the point $(\mathbf{r}, \mathbf{p})$. In Eq. A.4, we are actually talking about a subset of these particles which scatter to the new states $\mathbf{p}_1'$ and $\mathbf{p}_2'$. This subset only has a single corresponding impact parameter, because there is a one-one correspondence as discussed in Chapter 2. Since all of the momentum in the initial subset is transferred into the final states and vice versa for the reverse process, this is a statement of conservation of momentum. This means that the equality A.4 is satisfied by any additive quantity, which is conserved during a collision described by the states in Eq. A.4. For elastic collisions we have five such quantities, particle number, energy, and the three components of the net momentum. Therefore, a general form of $f(\mathbf{r}, \mathbf{p}, t)$ is given by,

$$\ln f(\mathbf{r}, \mathbf{p}, t) = a(\mathbf{r}) + 2\alpha(\mathbf{r}) \cdot \mathbf{P} - \beta(\mathbf{r}) \left(\frac{p^2}{2m} + U(\mathbf{r}) \right) \tag{A.5}$$

This is only a local condition, but by saying $f(\mathbf{r}, \mathbf{p}, t) = f(H_1)$ we enforce this everywhere (Eq. 3.1). Therefore, $\alpha = 0$ and a and β must be independent of position and we are left with

$$f(\mathbf{r}, \mathbf{p}, t) = \aleph \exp \left[-\beta \left(\frac{p^2}{2m} + U(\mathbf{r}) \right) \right] \tag{A.6}$$

where $\aleph$ is some normalization factor and it can be shown [13] for an ideal gas that $\beta = \frac{1}{k_B T}$, where T is the temperature of the system.

Appendix B

Calculation of Monte Carlo Collision Probabilities

Here we review the method used by Jackson and Zaremba to calculate collisions of test particles in their simulation of the condensate and thermal cloud [11], as it holds integral information for the implementation of this method. We also discuss an important aspect of the derivation, which is not discussed by Jackson and Zaremba. That is, there are two choice for the density in Eq. B.9, which lead to different results.

The mean collision rate of the physical atoms is decomposed by a MC method, which allows us to identify the test particles to the MC samples in such a way that leads to a collision probability.

From discussions in Section 2.5, it is clear that the collision integral,

$$C_{22}[f] = \int \frac{d^3p_2}{h^3} \int \frac{d\Omega}{4\pi} \sigma \frac{|\mathbf{p}_2 - \mathbf{p}|}{m} \left[(1+f)(1+f_2)f_3 f_4 - f f_2 (1+f_3)(1+f_4)\right], \tag{B.1}$$

describes collisions into and out of some phase-space region.

Following from the definitions made in Chapter 2 (definitions2.6), one has collision rate for the phase-space volume $d^3r d^3p$ about the point $(\mathbf{r}, \mathbf{p})$, which is given by

$$R_{22}^{out}(\mathbf{r}, \mathbf{p}, t) d^3r d^3p = \int \frac{d^3p_2}{h^3} \int \frac{d\Omega}{4\pi} \sigma \frac{|\mathbf{p}_2 - \mathbf{p}|}{m} f f_2 (1+f_3)(1+f_4) d^3r d^3p. \tag{B.2}$$

Thus, the mean collision rate for an atom in a cell of volume V_{cell}, is given by integrating over all possible momenta;

$$R_{22}^{out}(\mathbf{r}, t) V_{cell} = \int \frac{d^3p}{h^3} \int \frac{d^3p_2}{h^3} \int \frac{d\Omega}{4\pi} \sigma \frac{|\mathbf{p}_2 - \mathbf{p}|}{m} f f_2 (1+f_3)(1+f_4) V_{cell}. \tag{B.3}$$

Before applying the MC method to Eq. B.3, we pause to give the theoretical, equilibrium mean collision rate along the x axis, which is defined as

$$R_0^{22}(x) = \frac{n_0^t(x)}{\tau_0^{22}(x)}, \tag{B.4}$$

where $\tau_0^{22}(x)$ is the equilibrium local mean collision time and $n_0^t(x)$ is the equilibrium thermal cloud density. In the classical regime $\tau_0^{22}(x)$ reduces to

$$\frac{1}{\tau_0^{22}(x)} = \sqrt{2} n_0^t(x) \sigma v_{th}, \tag{B.5}$$

where v_{th} is the thermal mean speed, $v_{th} = \sqrt{\frac{8k_B T}{\pi m}}$. We will use this later in Chapter 5 to test the implementation of the results of this section.

Returning to Eq. B.3, we rewrite is as

$$R_{22}^{out}(\mathbf{r}, t) = \int \frac{d^3p}{h^3} \int \frac{d^3p_2}{h^3} f f_2 g(\mathbf{p}, \mathbf{p}_2, t) \equiv \int d^6p w(p, t) g(p, t), \tag{B.6}$$

remembering that $\mathbf{p}_3$ and $\mathbf{p}_4$ are functions of $\mathbf{p}$, $\mathbf{p}_2$ and Ω. The variable p is a point in the six-dimensional momentum space and $w(p, t)$ is called the weight function. If the integrand is non-zero on the domain $\left[-\frac{p_{max}}{2}, \frac{p_{max}}{2}\right]$ for each of the momentum components, one may use a MC method to give an approximate solution to the integral in Eq. B.6 as follows. Choose a point, p_i, in the momentum hyper volume $(p_{max})^6$, defined by the domain $\left[-\frac{p_{max}}{2}, \frac{p_{max}}{2}\right]$ for each momentum component, at random. Then choose another random number w_i in the range $[0, w_{max}]$, where w_{max} is the maximum value of the weight function. If $w_i < w(p_i, t)$, then the point p_i is accepted. Repeating this N times, one obtains an approximate solution to the integral given by

$$R_{22}^{out} \simeq (p_{max})^6 w_{max} \frac{1}{N} \sum_i^{N_{acc}} g(p_i^{acc}, t), \tag{B.7}$$

where the summation runs over all the accepted points. If it was such that $g = 1$, then the equivalent integral in Eq. B.6 is the square of the thermal cloud density, $n_t(\mathbf{r}, t)^2$. This would have the approximate solution,

$$n_t(\mathbf{r}, t)^2 \simeq (p_{max})^6 w_{max} \frac{N_{acc}}{N}, \tag{B.8}$$

where N_{acc} is the number of accepted points. This allows one to write

$$R_{22}^{out}(\mathbf{r}, t) \simeq n_t(\mathbf{r}, t)^2 \frac{1}{N_{acc}} \sum_i^{N_{acc}} g(p_i^{acc}, t), \tag{B.9}$$

where the summation of over the set of accepted points.

We now make the connection between these accepted points and the test particles of the simulation. The set of accepted points, p_i^{acc}, corresponds to N_{acc} $\mathbf{p}$ values and N_{acc} $\mathbf{p}_2$ values, distributed according to $f(\mathbf{r}, \mathbf{p}, t)$. Since, the test particles momenta are also distributed according to $f(\mathbf{r}, \mathbf{p}, t)$, one may associate the $2N_{acc}$ momentum sets with that of the test particles in the volume V_{cell}.

Jackson and Zaremba state that

> "If this set is to be representative of the local density, we must have $\tilde{n}(\mathbf{r}) = \frac{N_{cell}}{\Delta^3 r}$",

where $\tilde{n}(\mathbf{r})$ in our case is $n_t(\mathbf{r},t)$, $\Delta^3 r$ is the cell volume and the set refers to the test particles within the cell. It is unclear what is meant here, because $\frac{N_{cell}}{\Delta^3 r}$ is the density of the test particles. However, following the origins of $n_t(\mathbf{r},t)$, it is the thermal cloud density. Say we were to $n_t(\mathbf{r},t)$ as the thermal cloud density (which is done in Section 5.1), we would find that the collision integral, $C_{22}[f]$, is correctly sampled. I.e. we obtain the correct mean collision rate for the physical system. However, in doing this we are enforce the cloud of test particles to have the same mean collision rate for any number of test particles. This is clearly not what we want, because this leads to all sets of test particles, whether its 10,000 test particles or 10^{20} test particles, to undergo the same number of collisions over some time interval. As illustrated in Section 5.3, this results in the dynamics of the physical system we are simulating to be dependent on the number of test particles used in the simulation.

So what is the correct choice such that the dynamics of any number of test particles minic the dynamics of the physical atoms? We cannot use the case where both density terms $(n_t(\mathbf{r},t) \times n_t(\mathbf{r},t))$ are the density for the test particles, because is the same as saying that the physical system in question has the same number of atoms as test particles. Problem being that the dynamics of the system are dependent on the number of physical atoms, since we cannot factorize out the normalization of $f(\mathbf{r},\mathbf{p},t)$ in any of the equations of motion we are concerned with in this project. As it turns out, the correct choice is to use the thermal cloud density for one of the density terms and the test particle density for the other. I.e.

$$n_t(\mathbf{r},t)^2 \rightarrow n_t(\mathbf{r},t)\frac{N_{cell}}{V_{cell}}. \tag{B.10}$$

The justification of this can be seen via Eqs. 2.20 and 2.26, however, it is easily explained by the following. In representing the phase-space density, $f(\mathbf{r},\mathbf{p},t)$, by a swarm of test particles, we are representing each physical atom by $\frac{N_T}{N_p}$ test particles. Thus, if one physical atom undergoes a collision, the equivalent for the test particles is that $\frac{N_T}{N_p}$ test particles undergo a collision. We achieve this by multiplying Eq. B.9 by $\frac{N_T}{N_p}$, which is the equivalent of the statement in Eq. B.10.

Using Eq. B.10 one may write,

$$R_{22}^{out}(\mathbf{r},t)V_{cell} \simeq 2n_t(\mathbf{r},t)\sum_{(ij)}^{N_{acc}} g(\mathbf{p}^i,\mathbf{p}_2^j,t), \tag{B.11}$$

where the summation is over the particle pairs (ij), understanding that each test particle may only be pair with one other test particle. Thus, one may define the probability that pair, (ij), in the cell undergo a collision in the time interval Δt.

$$P_{ij}^{22}(\mathbf{r},t) \simeq n_t(\mathbf{r},t)\frac{|\mathbf{p}_i - \mathbf{p}_j|}{m}\int \frac{d\Omega}{4\pi}\sigma(1+f_3)(1+f_4)\Delta t \tag{B.12}$$

Here $g(\mathbf{p}^i,\mathbf{p}^j,t)$ has been replaced with the explicit formula and the factor of 2 from Eq. B.11 has been dropped, since, it's counting the fact that two test particles are involved in the collision. By defining this probability for pairs of test particles allows us to simulate collisions in a way which is consistent with the collision integral B.1.

Bibliography

[1] M. H. Anderson, J. R. Ensher, M. R. Matthews, C. E. Wieman, and E. A. Cornell, *Observation of Bose-Einstein condensation in a dilute atomic vapor*, Science **269** (1995), no. 5221, 198-201

[2] F. Dalfovo, S. Giorgini, L.P. Pitaevskii, and S. Stringari, *Theory of Bose-Einstein condensation in trapped gases*, Rev. Mod. Phys. **71** (1999), no. 3, 463-512

[3] P. B. Blakie, A. S. Bradley, M. J. Davis, R. J. Ballagh, and C. W. Gardiner, *Dynamics and statistical mechanics of ultra-cold Bose gases using c-field techniques*, Adv. Phys. **57** (2008), no. 5, 363-455

[4] A. Bezett and P. B. Blakie, *Projected Gross-Pitaevskii equation theory of finite-temperature collective modes for a trapped Bose gas*, Phys. Rev. A **79** (2009), no. 2, 023602

[5] D. S. Jin, M. R. Matthews, J. R. Ensher, C. E. Wieman, and E. A. Cornell, *Temperature-Dependent Damping and Frequency Shifts in Collective Excitations of a Dilute Bose-Einstein Condensate*, Phys. Rev. Lett. **78** (1997), no. 5, 764-767

[6] M. J. Bijlsma and H. T. C. Stoof, *Collisionless modes of a trapped Bose gas*, Phys. Rev. A **60** (1999), no. 5, 3973- 3981

[7] U. A. Khawaja and H. T. C. Stoof, *Kinetic theory of collective excitations and damping in Bose-Einstein condensed gases*, Phys. Rev. A **62** (2000), no. 5, 053602

[8] B. Jackson and E. Zaremba, *Quadrupole Collective Modes in Trapped Finite-Temperature Bose-Einstein Condensates*, Phys. Rev. Lett. **88** (2002), no. 18, 180402

[9] S. A. Morgan, M. Rusch, D. A. W. Hutchinson, and K. Burnett, *Quantitative Test of Thermal Field Theory for Bose-Einstein Condensates*, Phys. Rev. Lett. **91** (2003), no. 25, 250403

[10] E. Zaremba, T. Nikuni, and A. Griffin, *Dynamics of Trapped Bose Gases at Finite Temperatures*, J. Low Temp. Phys. **116** (1999), no. 3-4, 277-345

[11] B. Jackson and E. Zaremba, *Modeling Bose-Einstein condensed gases at finite temperatures with N-body simulations*, Phys. Rev. A **66** (2002), no. 3, 033606

[12] K. Huang, *Statistical Mechanics*, John Wiley and Sons, Inc., 1963

[13] M. Kardar, *Statistical Physics of Particles*, Cambridge University Press, 2007

[14] D. V. Schroeder, *An Introduction to Thermal Physics*, Addison Wesley Longman, 2000

[15] T. R. Kirkpatrick and J. R. Dorfman, *Transport theory for a weakly interacting condensed Bose gas*, Phys. Rev. A **28** (1983), no. 4, 2576-2579

[16] R. W. Hockney and J. W. Eastwood, *Computer Simulation Using Particles*, Taylor and Francis Group, 1988

[17] H. Yoshida, *RECENT PROGRESS IN THE THEORY AND APPLICATION OF SYMPLECTIC INTEGRATORS*, Celest. Mech. Dyn. Astron. **56** (1993), no. 1-2, 27-43

[18] E. Hairer, C. Lubich, and G. Wanner, *Geometric Numerical Integration: Structure-Preserving Algorithms for Ordinary Differential Equations Second Edition*, Springer, 2006

[19] C. K. Birdsall and A. B. Langdon, *Plasma Physics via Computer Simulation*, Adam Hilger, 1991

[20] D. Guéry-Odelin, F. Zambelli, J. Dalibard, and S. Stringari, *Collective oscillations of a classical gas confined in harmonic traps*, Phys. Rev. A **60** (1999), no. 6, 4851-4856

[21] S. K. Yip, *Magneto-optical absorption by electrons in the presence of parabolic confinement potentials*, Phys. Rev. B **43** (1991), no. 2, 1707-1718

[22] J. F. Dobson, *Harmonic-Potential Theorem: Implications for Approximate Many-Body Theories*, Phys. Rev. Lett. **73** (1994), no. 16, 2244-2247

[23] N. R. Thomas, N. Kjærgaard, P. S. Julienne, and A. C. Wilson, *Imaging of s and d Partial-Wave Interference in Quantum Scattering of Identical Bosonic Atoms*, Phys. Rev. Lett. **93**, no. 17, 173201

[24] A. S. Mellish, N. Kjærgaard, P. S. Julienne, and A. C. Wilson, *Quantum scattering of distinguishable bonsons using an ultracold-atom collider*, Phys. Rev. A **75**, no. 2, 020701

[25] A. A. Norrie, R. J. Ballagh, and C. W. Gardiner, *Quantum Turbulence in Condensate Collisions: An Application of the Classical Field Method*, Phys. Rev. Lett. **94**, no. 4, 040401

[26] M. Naraschewski and R. J. Glauber, *Spatial coherence and density correlations of trapped Bose gases*, Phys. Rev. A **59**, no. 6, 4595-4607

[27] R. J. Ballagh, *Lectures on "Computational methods for nonlinear partial differential equations"*, 25th September 2009, URL http://www.physics.otago.ac.nz/research/jackdodd/resources/comp_lectures_ballagh.html

[28] C. Buggle, J. Léonard, W. von Klitzing, and J. T. M. Walraven, *Interferometric Determination of the s and* d-*Wave Scattering Amplitudes in* ^{87}Rb, Phys. Rev. Lett. **93**, no. 17, 173202